B
R
L

CONTRACT REPORT BRL-CR-535

A SOLUTION METHOD FOR NONLINEAR DYNAMIC ANALYSIS OF SHELL STRUCTURES

Prepared by

Massachusetts Institute of Technology
Mechanical Engineering Department
Cambridge, Massachusetts 02139

October 1984

US ARMY BALLISTIC RESEARCH LABORATORY
ABERDEEN PROVING GROUND, MARYLAND

Destroy this report when it is no longer needed.
Do not return it to the originator.

Additional copies of this report may be obtained from the National Technical Information Service, U. S. Department of Commerce, Springfield, Virginia 22161.

The findings in this report are not to be construed as an official Department of the Army position, unless so designated by other authorized documents.

The use of trade names or manufacturers' names in this report does not constitute indorsement of any commercial product.

UNCLASSIFIED

SECURITY CLASSIFICATION OF THIS PAGE *(When Data Entered)*

REPORT DOCUMENTATION PAGE

READ INSTRUCTIONS BEFORE COMPLETING FORM

1. REPORT NUMBER: CONTRACT REPORT BRL-CR-535	2. GOVT ACCESSION NO.
3. RECIPIENT'S CATALOG NUMBER	
4. TITLE *(and Subtitle)*: A Solution Method for Nonlinear Dynamic Analysis of Shell Structures	5. TYPE OF REPORT & PERIOD COVERED: Contract Report May 1982 to June 1983
	6. PERFORMING ORG. REPORT NUMBER
7. AUTHOR(s): Klaus-Jurgen Bathe	8. CONTRACT OR GRANT NUMBER(s): DAAK11-82-K-0005
9. PERFORMING ORGANIZATION NAME AND ADDRESS: Mechanical Engineering Department, Massachusetts Institute of Technology, Cambridge, MA 02139	10. PROGRAM ELEMENT, PROJECT, TASK AREA & WORK UNIT NUMBERS: 1L61102AH43
11. CONTROLLING OFFICE NAME AND ADDRESS: US Army Ballistic Research Laboratory, ATTN: AMXBR-OD-ST, Aberdeen Proving Ground, MD 21005-5066	12. REPORT DATE: October 1984
	13. NUMBER OF PAGES: 56
14. MONITORING AGENCY NAME & ADDRESS *(if different from Controlling Office)*	15. SECURITY CLASS. *(of this report)*: UNCLASSIFIED
	15a. DECLASSIFICATION/DOWNGRADING SCHEDULE

16. DISTRIBUTION STATEMENT *(of this Report)*

Approved for public release: distribution unlimited.

17. DISTRIBUTION STATEMENT *(of the abstract entered in Block 20, if different from Report)*

18. SUPPLEMENTARY NOTES

This work was funded and technically monitored by the Blast Dynamics Branch, Terminal Ballistics Division, AMXBR-TBD, Dr. Joseph M. Santiago, Contracting Officer's Representative.

19. KEY WORDS *(Continue on reverse side if necessary and identify by block number)*

Quadilateral Shell Element
Finite Element Structural Analysis
Geometric and Material Nonlinearities
Degenerate 3-D Isoparametric Formulation
ADINA Finite Element Program
Static and Dynamic Response

20. ABSTRACT *(Continue on reverse side if necessary and identify by block number)*

A new four-node (non-flat) general quadrilateral shell element for geometric and material static and dynamic nonlinear analysis is presented. The element is formulated using three-dimensional continuum mechanics theory and it is applicable to the analysis of thin and thick shells. The formulation of the element and the solutions to various test and demonstrative example problems are presented and discussed.

DD FORM 1 JAN 73 1473 EDITION OF 1 NOV 65 IS OBSOLETE

UNCLASSIFIED

SECURITY CLASSIFICATION OF THIS PAGE *(When Data Entered)*

TABLE OF CONTENTS

LIST OF ILLUSTRATIONS

LIST OF ILLUSTRATIONS

1. INTRODUCTION

The finite element analysis of general shell structures has been a very active field of research for a large number of years [14, 29]. However, despite the fact that many different shell elements have already been proposed, the search for a shell element capable of representing the general nonlinear behavior of shells with arbitrary geometry and loading conditions in an effective and reliable manner is still continuing very actively.

During recent years it has become apparent that two approaches for the development of shell elements are very appropriate:

- The use of simple elements, based on the discrete-Kirchhoff approach for the analysis of thin shells [2, 5 - 9].
- The use of degenerated isoparametric elements in which fully three-dimensional stress and strain conditions are degenerated to shell behavior [2, 3, 5, 7, 17, 19, 24, 29].

The latter approach has the advantage of being independent of any particular shell theory, and this approach was used in ref. [3] to formulate a general shell element for geometric and material nonlinear analysis. This element has been employed very successfully when used with 9 or, in particular, 16 nodes. However, the 16-node element is quite expensive, and although it is possible to use in some analyses only a few elements to represent the total structure (see Sections 4.2 and 4.5), in other analyses still a fairly large number of elements need be employed [5].

Considering general shell analyses, much emphasis has been placed onto the development of a versatile, reliable and cost-effective 4-node shell element [16, 17, 22, 28]. Such element would complement the above high-order 16-node element and may be more effective in certain analyses. The difficulties in the development of such element lie in that the element should be applicable in a reliable manner to thin and thick shells of arbitrary geometries for general nonlinear analysis.

The objective in this paper is to present a simple 4-node general shell element with the following properties:

- the element is formulated using three-dimensional stress and strain conditions without use of a shell theory;
- the element is applicable to thin and thick shells and can be employed to model arbitrary geometries;

- the element is applicable to the conditions of large displacements and rotations but small strains, and can be used effectively in materially nonlinear analysis.

The formulation of the element is quite simple and transparent, and the element has good predictive capability without containing spurious zero energy modes.

In the next section of the paper we discuss some basic considerations with respect to the assumptions used, and in Section 3 we present the element formulation for nonlinear analysis. The results obtained in numerical solutions that demonstrate the properties of the element are given in Section 4.

2. BASIC CONSIDERATIONS

The formulation of the 4-node shell element represents an extension of the shell element discussed in refs. [2, 3], and we therefore use the same notation as in those references. Also, to focus attention onto some key issues of the formulation, we consider in this section only linear analysis conditions.

The geometry of the element, see Fig. 1, is described using [2, p. 255]:

$$ {}^{\ell}x_i = \sum_{k=1}^{4} h_k \, {}^{\ell}x_i^k + \frac{r_3}{2} \sum_{k=1}^{4} a_k h_k \, {}^{\ell}V_{ni}^k \qquad (1) $$

where the $h_k(r_1,r_2)$ are the two-dimensional interpolation functions corresponding to node k; the r_i are the natural coordinates; and

${}^{\ell}x_i$ = Cartesian coordinates of any point in the element;

${}^{\ell}x_i^k$ = Cartesian coordinates of nodal point k;

${}^{\ell}V_{ni}^k$ = Components of director vector at node k (which is not necessarily normal to the midsurface of the element);

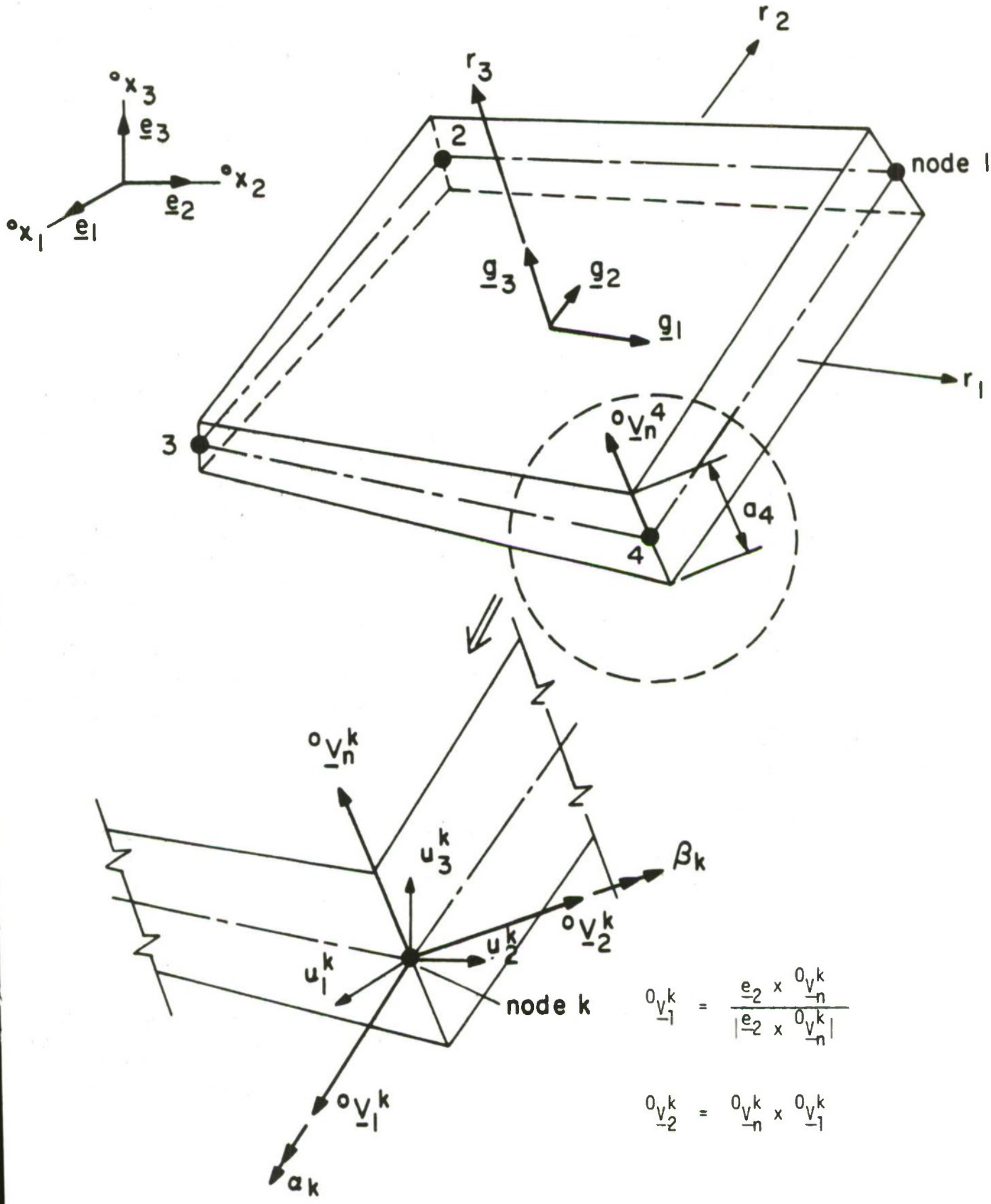

$$ {}^{0}\underline{v}_{1}^{k} = \frac{\underline{e}_2 \times {}^{0}\underline{v}_{n}^{k}}{|\underline{e}_2 \times {}^{0}\underline{v}_{n}^{k}|} $$

$$ {}^{0}\underline{v}_{2}^{k} = {}^{0}\underline{v}_{n}^{k} \times {}^{0}\underline{v}_{1}^{k} $$

Figure 1 Four-node shell element

and a_k is the shell thickness at node k, measured along the vector ${}^{\ell}\underline{V}_n^k$. The left superscript is zero for the initial geometry of the element and is equal to 1 for the deformed element geometry. Note that the thickness of the element varies and the element is in general non-flat.

The displacements of any particle with natural coordinates r_i of the shell element in the stationary Cartesian coordinate system are:

$$u_i = \sum_{k=1}^{4} h_k u_i^k + \frac{r_3}{2} \sum_{k=1}^{4} a_k h_k \left(- {}^{0}V_{2i}^k \alpha_k + {}^{0}V_{1i}^k \beta_k\right) \qquad (2)$$

where the u_i^k are the nodal point displacements into the Cartesian coordinate directions, and the α_k and β_k are the rotations of the director vector ${}^{0}\underline{V}_n^k$ about the ${}^{0}\underline{V}_1^k$ and ${}^{0}\underline{V}_2^k$ axes (see Fig. 1).

A basic problem inherent in the use of the above interpolation of the displacements, and the derivation of the strain-displacement matrices therefrom, is that the element "locks" when it is thin. This is due to the fact that with these interpolations the transverse shear strains cannot vanish at all points in the element, when it is subjected to a constant bending moment. Hence, although the basic continuum mechanics assumptions contain the Kirchhoff shell assumptions, the finite element discretization is not able to represent these assumptions, rendering the element not applicable to the analysis of thin plates or shells (see [2, p. 240] and [5, 7]). To solve this deficiency, various remedies based on selective and reduced integration have been proposed [17, 22, 23] but there is still much room for more effective and reliable elements for general nonlinear analysis.

Considering our element formulation — because the problem lies in the representation of the transverse shear strains — we proceed to not evaluate these shear strains from the displacements in Eq. (2) but to introduce separate interpolations for these strain components. Since we consider non-flat shell elements, the separate interpolations are performed effectively in a convected coordinate system.(†)

(†) Note that in refs. [2] and [3], the shell element formulation is discussed in the global stationary coordinate system, because all displacement components are interpolated in the same way. To emphasize that we use here stress and strain measures in the convected coordinate system, we place a curl (~) over these quantities.

The choice of the interpolation for the transverse shear strain components is the key assumption in our element formulation, because adequate coupling between the element displacements and rotations must be introduced and the element should not exhibit any spurious zero energy modes. For our element we use, see Fig. 2,

$$\tilde{\varepsilon}_{13} = \frac{1}{2}(1 + r_2)\,\tilde{\varepsilon}^{A}_{13} + \frac{1}{2}(1 - r_2)\,\tilde{\varepsilon}^{C}_{13}$$

$$\tilde{\varepsilon}_{23} = \frac{1}{2}(1 + r_1)\,\tilde{\varepsilon}^{D}_{23} + \frac{1}{2}(1 - r_1)\,\tilde{\varepsilon}^{B}_{23} \quad . \tag{3}$$

Since the kinematic relations for the above shear strains are not satisfied using Eq. (3), we impose them using Lagrange multipliers [2, 27] to obtain

$$\Pi^{*} = \frac{1}{2}\int_{V} \tilde{\tau}^{ij}\,\tilde{\varepsilon}_{ij}\,dV + \int_{V} \lambda^{13}\,(\tilde{\varepsilon}_{13} - \tilde{\varepsilon}^{DI}_{13})\,dV$$

$$+ \int_{V} \lambda^{23}\,(\tilde{\varepsilon}_{23} - \tilde{\varepsilon}^{DI}_{23})\,dV - W \tag{4}$$

where the $\tilde{\tau}^{ij}$ are the contravariant components of the Cauchy stress tensor [13, 15], the $\tilde{\varepsilon}_{ij}$ are the covariant components of the infinitesimal strain tensor, the λ^{13} and λ^{23} are the Lagrange multipliers, the $\tilde{\varepsilon}^{DI}_{13}$ and $\tilde{\varepsilon}^{DI}_{23}$ are the transverse shear strains evaluated using the displacement interpolations in Eq. (2), and W is the potential of the external loads. For the Lagrange multipliers we choose the following interpolations,

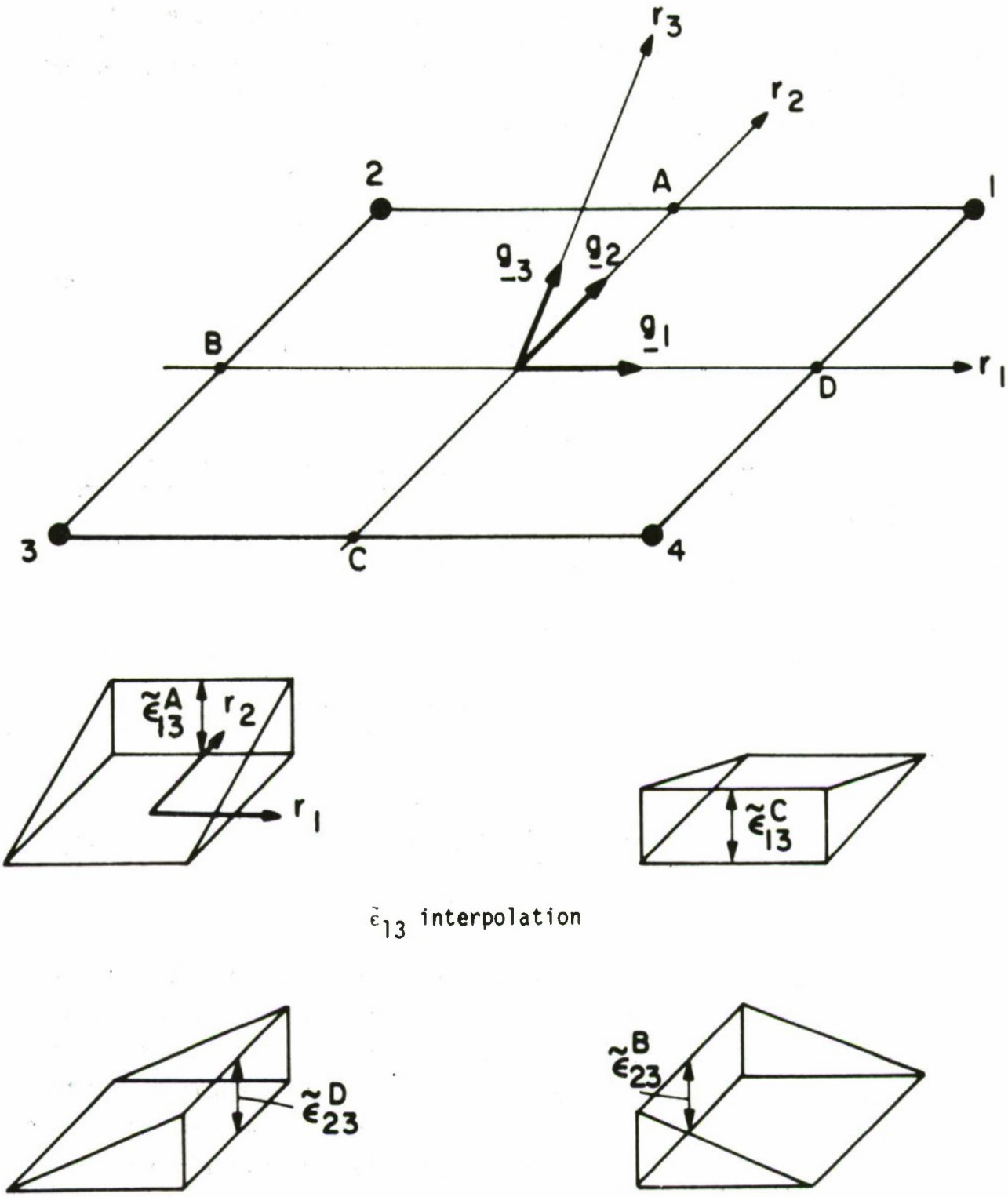

Figure 2 Interpolation functions for the transverse shear strains

$$\lambda^{13} = \lambda^{A}\,\delta(r_1)\,\delta(1 - r_2) + \lambda^{C}\,\delta(r_1)\,\delta(1 + r_2)$$

$$\lambda^{23} = \lambda^{D}\,\delta(r_2)\,\delta(1 - r_1) + \lambda^{B}\,\delta(r_2)\,\delta(1 + r_1) \tag{5}$$

where $\delta(...)$ is the Dirac-delta function. This represents a weakening of the Lagrange multiplier constraint in Eq. (4) [10]. Substituting from Eq. (5) into Eq. (4) and invoking that $\delta\Pi^* = 0$ gives the distinct constraints

$$\tilde{\varepsilon}_{13} = \tilde{\varepsilon}^{DI}_{13}\Big|_{\text{at A}} \qquad \tilde{\varepsilon}_{13} = \tilde{\varepsilon}^{DI}_{13}\Big|_{\text{at C}}$$

$$\tilde{\varepsilon}_{23} = \tilde{\varepsilon}^{DI}_{23}\Big|_{\text{at D}} \qquad \tilde{\varepsilon}_{23} = \tilde{\varepsilon}^{DI}_{23}\Big|_{\text{at B}} \tag{6}$$

Hence, the complete element stiffness matrix is calculated using the functional

$$\Pi^{*} = \frac{1}{2}\int_{V} \tilde{\tau}^{ij}\,\tilde{\varepsilon}_{ij}\,dV - W \tag{7}$$

with stress and strain components in convected coordinates and

- Eqs. (1) and (2) to evaluate the strain components $\tilde{\varepsilon}_{11}$, $\tilde{\varepsilon}_{22}$ and $\tilde{\varepsilon}_{12}$;
- Eq. (3) to evaluate the strain components $\tilde{\varepsilon}_{13}$, $\tilde{\varepsilon}_{23}$; and
- Eq. (6) to express the variables $\tilde{\varepsilon}^{A}_{13}$, $\tilde{\varepsilon}^{C}_{13}$, $\tilde{\varepsilon}^{D}_{23}$ and $\tilde{\varepsilon}^{B}_{23}$ in terms of the nodal point displacements and rotations of Eq. (2).

Considering the representation that we have chosen for the transverse shear strains, we can make the following three important observations:

1) The element is able to represent the six rigid body modes.

The element contains the rigid body modes because zero strains are calculated in the formulation when the element nodal point displacements and rotations correspond to an element rigid body displacement. This can be verified by using Eqs. (1) to (6) to evaluate the strains, but more easily we can use the fact that the 4-node shell element of ref. [3] satisfies the rigid body mode criterion. Hence, for a rigid body displacement the $\tilde{\varepsilon}_{13}^{DI}$ and $\tilde{\varepsilon}_{23}^{DI}$ are zero, from which it follows that also the shear strains in Eq. (3) are zero, and the rigid body mode criterion is satisfied.

2) The element can approximate the Kirchhoff-Love hypothesis of negligible shear deformation effects and can be used for thin shells.

Various demonstrative solutions are given in Section 4.

3) Based on our studies the element does not contain any spurious zero energy modes (using a "full" numerical integration).

We reach this observation by studying the strains along the element sides. If the element were to contain a spurious zero energy mode, the strains along every side should vanish for a displacement pattern (to be identified) other than the displacements corresponding to a true rigid body mode. However, such displacement pattern could not be identified.

Considering the practical use of the element the interpolation employed for the transverse shear strains shows that $\tilde{\varepsilon}_{13}$ is constant with r_1 and in general discontinuous at $r_1 = \pm 1$ (between elements), and similarly $\tilde{\varepsilon}_{23}$ is constant with r_2 and in general discontinuous at $r_2 = \pm 1$. As a consequence, the accuracy with which transverse shear stresses are predicted depends to a significant degree on the mesh used and the geometric distortions of the elements. However, our experience is that the bending stress predictions are relatively little affected by element distortions (see Section 4).

To employ Eq. (7), we also need to use the appropriate constitutive relations:

$$\tilde{\tau}^{ij} = \tilde{C}^{ijkl}\tilde{\varepsilon}_{kl} \tag{8}$$

where $\tilde{C}^{ijkl}$ is the fourth-order contravariant constitutive tensor in the convected coordinates r_i. The constitutive law is known in the local Cartesian system of orthonormal base vectors $\hat{\underline{e}}_i$, i = 1, 2, 3, with the condition $\hat{\tau}^{33}$ equal to zero, see Fig. 3 (refer to [2], p. 258). Denoting this constitutive tensor by $\tilde{C}^{mnop}$, the constitutive tensor for Eq. (8) is obtained using the transformation

$$\tilde{C}^{ijkl} = (\underline{g}^i \cdot \hat{\underline{e}}_m)\ (\underline{g}^j \cdot \hat{\underline{e}}_n)\ (\underline{g}^k \cdot \hat{\underline{e}}_o)\ (\underline{g}^\ell \cdot \hat{\underline{e}}_p)\ \hat{C}^{mnop} \qquad (9)$$

where the $\underline{g}^i$ are the contravariant base vectors of the convected coordinates r_i. These vectors are calculated using the covariant base vectors $\underline{g}_i$, where

$$\underline{g}_i = \frac{\partial \underline{O}_x}{\partial r_i} \qquad (10)$$

with $\underline{O}_x$ from Eq. (1) and the following relations,

$$g_{ij} = \underline{g}_i \cdot \underline{g}_j \qquad (11)$$

and

$$\underline{g}^i = g^{ij}\ \underline{g}_j$$

$$g^{ij} = \frac{D^{ij}}{|\underline{J}|^2} \qquad (12)$$

where D^{ij} is the cofactor of the term g_{ij} in the matrix of the metric tensor and $|\underline{J}|$ is the determinant of the Jacobian matrix at the point considered.

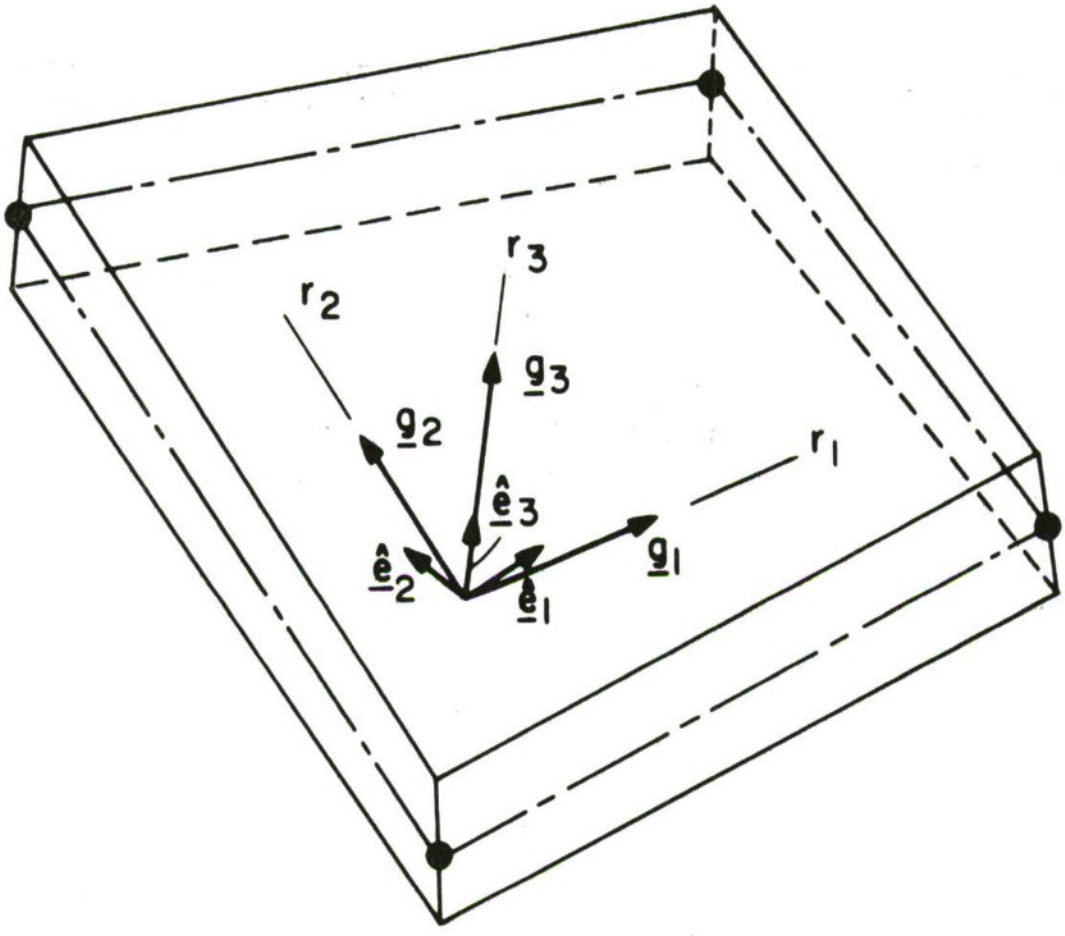

$$\hat{e}_3 = \frac{g_3}{|g_3|} \quad ; \quad \hat{e}_1 = \frac{g_2 \times \hat{e}_3}{|g_2 \times \hat{e}_3|} \quad ; \quad \hat{e}_2 = \hat{e}_3 \times \hat{e}_1$$

Figure 3 Local Cartesian coordinate system used

3. TOTAL LAGRANGIAN FORMULATION

The large displacement formulation of the shell element is based on the derivation given in ref. [2, Section 6.3.5], and the concepts and interpolations presented in the previous section.

The geometry of the element at any time t is defined as in Eq. (1) but using the nodal point coordinates, ${}^{t}x_i^k$, and director vectors ${}^{t}\underline{V}_n^k$, at time t,(÷)

$$ {}^{t}x_i = h_k \; {}^{t}x_i^k + \frac{r_3}{2} a_k \, h_k \; {}^{t}V_{ni}^k \tag{13} $$

where we imply summation over k. The displacements, ${}^{t}u_i$, and incremental displacements, u_i, of a particle of the element at time t are hence given by

$$ \begin{aligned} {}^{t}u_i &= h_k \; {}^{t}u_i^k + \frac{r_3}{2} \; a_k \, h_k \, ({}^{t}V_{ni}^k - {}^{0}V_{ni}^k) \\ u_i &= h_k \, u_i^k + \frac{r_3}{2} a_k \, h_k \, (-{}^{t}V_{2i}^k \, \alpha_k + {}^{t}V_{1i}^k \, \beta_k) \end{aligned} \tag{14} $$

where the ${}^{t}u_i^k$ are the nodal point displacements at time t, the u_i^k are the incremental nodal point displacements from the configuration at time t, and the variables ${}^{t}V_{2i}^k$, ${}^{t}V_{1i}^k$, α_k and β_k are defined as in Eq. (2) but referred to the configuration at time t.

This kinematic description implies the following hypotheses:

- The director vectors remain straight during the deformations.
- The "thickness" of the element measured along the director vectors remains constant during the deformations; hence only small strain conditions are considered.

Using the assumptions in Eqs. (13) and (14) the geometric and material nonlinear response is analyzed using an incremental formulation [2], in which the configuration is sought for time (load step) "t + Δt", when the configuration for time "t" is known. The basis of this incremental

(÷) Note that the superscript t on a variable denotes the configuration at time t in the incremental solution and does not imply a dynamic analysis.

formulation is the use of the virtual work principle applied to the configuration at time $t+\Delta t$. In essence, two approaches can be employed leading to the updated Lagrangian and the total Lagrangian formulations. These approaches are, from a continuum mechanics point of view, equivalent, and in the following we develop the governing finite element relations for the total Lagrangian formulation.

The principle of virtual work applied to the configuration at time $t+\Delta t$ is

$$\int_{{}^0V} {}^{t+\Delta t}_{0}\tilde{S}^{ij} \, \delta {}^{t+\Delta t}_{0}\tilde{\varepsilon}_{ij} \, {}^0dV = {}^{t+\Delta t}R \tag{15}$$

where the ${}^{t+\Delta t}_{0}\tilde{S}^{ij}$ are the contravariant components of the second Piola-Kirchhoff stress tensor at time $t+\Delta t$ and referred to the configuration at time 0, and the ${}^{t+\Delta t}_{0}\tilde{\varepsilon}_{ij}$ are the covariant components of the Green-Lagrange strain tensor at time $t+\Delta t$ and referred to time 0. Both sets of tensor components are measured in the convected coordinate system r_i, $i = 1,2,3$. The external virtual work is given by ${}^{t+\Delta t}R$ and includes the work due to the applied surface tractions and body forces.

For the incremental solution, the stresses and strains are decomposed into the known quantities, ${}^{t}_{0}\tilde{S}^{ij}$ and ${}^{t}_{0}\tilde{\varepsilon}_{ij}$, and unknown increments, ${}_0\tilde{S}^{ij}$ and ${}_0\tilde{\varepsilon}_{ij}$, so that

$${}^{t+\Delta t}_{0}\tilde{S}^{ij} = {}^{t}_{0}\tilde{S}^{ij} + {}_0\tilde{S}^{ij} \tag{16}$$

$${}^{t+\Delta t}_{0}\tilde{\varepsilon}_{ij} = {}^{t}_{0}\tilde{\varepsilon}_{ij} + {}_0\tilde{\varepsilon}_{ij} \, . \tag{17}$$

In addition, the strain increment can be written as a linear part, ${}_0\tilde{e}_{ij}$, and a nonlinear part, ${}_0\tilde{\eta}_{ij}$, hence

$$ {}_0\tilde{\varepsilon}_{ij} = {}_0\tilde{e}_{ij} + {}_0\tilde{\eta}_{ij} \quad . \tag{18} $$

Substituting from Eqs. (16) to (18) into Eq. (15) and using the linearized expressions ${}_0\tilde{S}^{ij} = {}_0\tilde{C}^{ijkl}\ {}_0\tilde{e}_{kl}$ and $\delta\,{}_0\tilde{\varepsilon}_{ij} = \delta\,{}_0\tilde{e}_{ij}$, we obtain the linearized equation of motion

$$ \int_{{}^0V} {}_0\tilde{C}^{ijkl}\ {}_0\tilde{e}_{kl}\ \delta\,{}_0\tilde{e}_{ij}\ {}^0dV + \int_{{}^0V} {}^t_0\tilde{S}^{ij}\ \delta\,{}_0\tilde{\eta}_{ij}\ {}^0dV $$

$$ = {}^{t+\Delta t}R - \int_{{}^0V} {}^t_0\tilde{S}^{ij}\ \delta\,{}_0\tilde{e}_{ij}\ {}^0dV \quad . \tag{19} $$

This equation is the basic equilibrium relation employed to develop the governing finite element matrices. For the actual solution of problems, it is frequently important to use equilibrium iterations, but the finite element matrices and vectors used in these iterations can be derived directly from the matrices obtained using Eq. (19) [2]. Note that ${}_0\tilde{C}^{ijkl}$ is now obtained using Eq. (9) with the condition ${}^t_0\hat{S}^{33} = 0$, which implies the more natural condition ${}^t\hat{\tau}^{33} = 0$ only in the small strain case.

The basic problem of the finite element discretization of Eq. (19) lies in expressing the strain terms of Eq. (19) in terms of the finite element interpolations. Using the definition of the Green-Lagrange strain components

$$ {}^t_0\tilde{\varepsilon}_{ij} = \frac{1}{2}\left({}^t\underline{g}_i \cdot {}^t\underline{g}_j - {}^0\underline{g}_i \cdot {}^0\underline{g}_j\right) \tag{20} $$

and the relations in Eqs. (13) and (14) we obtain

$$ {}^{0}\tilde{e}_{ii} = h_{k,i}\ {}^{t}\underline{g}_i \cdot \underline{u}_k + \frac{r_3}{2} a_k h_{k,i} \left(-\alpha_k\ {}^{t}\underline{g}_i \cdot {}^{t}\underline{v}_2^k + \beta_k\ {}^{t}\underline{g}_i \cdot {}^{t}\underline{v}_1^k\right) \qquad (21\text{-a}) $$

$$ {}^{0}\tilde{\eta}_{ii} = \frac{1}{2} h_{k,i}\, h_{p,i}\ \underline{u}_k \cdot \underline{u}_p + \frac{r_3}{2} h_{k,i}\, h_{p,i}\, a_p \left(-\alpha_p\ {}^{t}\underline{v}_2^p \cdot \underline{u}_k + \beta_p\ {}^{t}\underline{v}_1^p \cdot \underline{u}_k\right) $$

$$ + \frac{(r_3)^2}{8} h_{k,i}\, h_{p,i}\, a_k\, a_p \left(-\alpha_k\ {}^{t}\underline{v}_2^k + \beta_k\ {}^{t}\underline{v}_1^k\right) \cdot \left(-\alpha_p\ {}^{t}\underline{v}_2^p + \beta_p\ {}^{t}\underline{v}_1^p\right) \qquad (21\text{-b}) $$

$$ (i = 1,2) $$

with the notation $h_{k,i} = \dfrac{\partial h_k}{\partial r_i}$, $\underline{u}_k^T = [u_1^k \quad u_2^k \quad u_3^k]$, and

$$ {}^{0}\tilde{e}_{12} = \frac{1}{2} \Big[h_{k,2}\ {}^{t}\underline{g}_1 \cdot \underline{u}_k + h_{k,1}\ {}^{t}\underline{g}_2 \cdot \underline{u}_k + $$

$$ \frac{r_3}{2} h_{k,2}\ a_k \left(-\alpha_k\ {}^{t}\underline{v}_2^k \cdot {}^{t}\underline{g}_1 + \beta_k\ {}^{t}\underline{v}_1^k \cdot {}^{t}\underline{g}_1\right) + $$

$$ \frac{r_3}{2} h_{k,1}\ a_k \left(-\alpha_k\ {}^{t}\underline{v}_2^k \cdot {}^{t}\underline{g}_2 + \beta_k\ {}^{t}\underline{v}_1^k \cdot {}^{t}\underline{g}_2\right) \Big] \qquad (22\text{-a}) $$

$$ {}^{0}\tilde{\eta}_{12} = \frac{1}{2} \Big[h_{k,1}\, h_{p,2}\ \underline{u}_k \cdot \underline{u}_p + $$

$$ \frac{r_3}{2} h_{k,1}\, h_{p,2}\ a_p \left(-\alpha_p\ {}^{t}\underline{v}_2^p \cdot \underline{u}_k + \beta_p\ {}^{t}\underline{v}_1^p \cdot \underline{u}_k\right) + $$

$$ \frac{r_3}{2} h_{k,1}\, h_{p,2}\ a_k \left(-\alpha_k\ {}^{t}\underline{v}_2^k \cdot \underline{u}_p + \beta_k\ {}^{t}\underline{v}_1^k \cdot \underline{u}_p\right) + $$

$$ \frac{(r_3)^2}{4} h_{k,1}\, h_{p,2}\, a_k\, a_p \left(-\alpha_k\ {}^{t}\underline{v}_2^k + \beta_k\ {}^{t}\underline{v}_1^k\right) \cdot \left(-\alpha_p\ {}^{t}\underline{v}_2^p + \beta_p\ {}^{t}\underline{v}_1^p\right) \Big] $$

(22-b)

Further, we obtain for the transverse shear strains, using Eqs. (3) and (6),

$$
\begin{aligned}
{}^{0}\tilde{e}_{13} = \frac{1}{8}(1+r_2)\Big[& {}^{t}g^{A}_{3i}\,(u_i^1 - u_i^2) + \frac{1}{2}\,{}^{t}g^{A}_{1i}\,(-\alpha_1 a_1\,{}^{t}V^1_{2i} + \beta_1 a_1\,{}^{t}V^1_{1i} \\
& - \alpha_2 a_2\,{}^{t}V^2_{2i} + \beta_2 a_2\,{}^{t}V^2_{1i})\Big] \\
+ \frac{1}{8}(1-r_2)\Big[& {}^{t}g^{C}_{3i}\,(u_i^4 - u_i^3) + \frac{1}{2}\,{}^{t}g^{C}_{1i}\,(-\alpha_4 a_4\,{}^{t}V^4_{2i} + \beta_4 a_4\,{}^{t}V^4_{1i} \\
& - \alpha_3 a_3\,{}^{t}V^3_{2i} + \beta_3 a_3\,{}^{t}V^3_{1i})\Big]
\end{aligned}
\qquad (23\text{-a})
$$

$$
\begin{aligned}
{}^{0}\tilde{\eta}_{13} = \frac{1}{32}(1+r_2)\Big[& (-\alpha_1 a_1\,{}^{t}V^1_{2i} + \beta_1 a_1\,{}^{t}V^1_{1i} - \alpha_2 a_2\,{}^{t}V^2_{2i} + \beta_2 a_2\,{}^{t}V^2_{1i}) \\
& (u_i^1 - u_i^2)\Big] \\
+ \frac{1}{32}(1-r_2)\Big[& (-\alpha_4 a_4\,{}^{t}V^4_{2i} + \beta_4 a_4\,{}^{t}V^4_{1i} - \alpha_3 a_3\,{}^{t}V^3_{2i} + \beta_3 a_3\,{}^{t}V^3_{1i})\,(u_i^4 - u_i^3)\Big]
\end{aligned}
\qquad (23\text{-b})
$$

and,

$$
\begin{aligned}
{}^{0}\tilde{e}_{23} = \frac{1}{8}(1+r_1)\Big[& {}^{t}g^{D}_{3i}\,(u_i^1 - u_i^4) + \frac{1}{2}\,g^{D}_{2i}\,(-\alpha_1 a_1\,{}^{t}V^1_{2i} + \beta_1 a_1\,{}^{t}V^1_{1i} \\
& - \alpha_4 a_4\,{}^{t}V^4_{2i} + \beta_4 a_4\,{}^{t}V^4_{1i})\Big] \\
+ \frac{1}{8}(1-r_1)\Big[& {}^{t}g^{B}_{3i}\,(u_i^2 - u_i^3) + \frac{1}{2}\,{}^{t}g^{B}_{2i}\,(-\alpha_2 a_2\,{}^{t}V^2_{2i} + \beta_2 a_2\,{}^{t}V^2_{1i} \\
& - \alpha_3 a_3\,{}^{t}V^3_{2i} + \beta_3 a_3\,{}^{t}V^3_{1i})\Big]
\end{aligned}
\qquad (24\text{-a})
$$

$$
{}^{0}\tilde{\eta}_{23} = \frac{1}{32}(1+r_1)\left[(-\alpha_1 a_1\, {}^{t}V^{1}_{2i} + \beta_1 a_1\, {}^{t}V^{1}_{1i} - \alpha_4 a_4\, {}^{t}V^{4}_{2i} + \beta_4 a_4\, {}^{t}V^{4}_{1i})(u^{1}_{i} - u^{4}_{i})\right]
$$

$$
+ \frac{1}{32}(1-r_1)\left[(-\alpha_2 a_2\, {}^{t}V^{2}_{2i} + \beta_2 a_2\, {}^{t}V^{2}_{1i} - \alpha_3 a_3\, {}^{t}V^{3}_{2i} + \beta_3 a_3\, {}^{t}V^{3}_{1i})(u^{2}_{i} - u^{3}_{i})\right]. \tag{24-b}
$$

Note that, since we assume the thickness of the shell to be constant, the strain ${}^{t}_{0}\tilde{\varepsilon}_{33}$ through the element thickness is zero.

The expressions in Eqs. (21) to (24) are substituted into Eq. (19) which in the standard manner yields the linear strain incremental stiffness matrix ${}^{t}_{0}\underline{K}_{L}$, the nonlinear strain (or geometric) incremental stiffness matrix ${}^{t}_{0}\underline{K}_{NL}$ and the nodal point force vector ${}^{t}_{0}\underline{F}$ in the finite element incremental equilibrium relations [2],

$$
({}^{t}_{0}\underline{K}_{L} + {}^{t}_{0}\underline{K}_{NL})\,\underline{u} = {}^{t+\Delta t}\underline{R} - {}^{t}_{0}\underline{F} \quad . \tag{25}
$$

The element matrices in Eq. (25) correspond to five degrees of freedom per node, see Fig. 1, but in some applications it is convenient to use instead of α_k and β_k three rotations about the global coordinate axes (see Section 4.6). In this case, we simply transform the matrices of Eq. (25) in the standard manner [2].

The element developed can be used for nonlinear dynamic analysis of shells with any time integration method [2], using a consistent mass matrix calculated in the standard way or a lumped mass matrix with the diagonal terms $m_{ii} = \frac{{}^{0}\rho\,{}^{0}V}{4}$ and $m_{jj} = \frac{{}^{0}\rho\,{}^{0}V}{16}(a_k)^2$ for translational and rotational degrees of freedom, respectively.

4. NUMERICAL TESTS AND EXAMPLE SOLUTIONS

We have implemented our shell element in the ADINA computer program and have performed various numerical tests to study the predictive capabilities of the element. The following solutions were all obtained using 2x2 Gauss integration in the $r_3 = 0$ surface of the element, and 2 and 4 point Gauss integration in the r_3 direction, for elastic and elasto-plastic analyses, respectively.

4.1 Some simple tests

As a first step to test the element, the eigenvalues of the stiffness matrices of undistorted and distorted elements were calculated. In all cases, as expected, the element displayed the six rigid body modes and no spurious zero energy modes.

4.1.a Patch tests

For the patch test [2, 18] the mesh shown in Fig. 4 was used. In the first analysis the mesh was loaded with the constant moment indicated, and a constant curvature (linear distribution of rotations) was obtained for both plate thickness in the two plate directions. The transverse displacements predicted by the model were — as expected — those of Kirchhoff-Love plate theory at nodes 7 and 8.

In the second analysis the rotational degrees of freedom were deleted and the mesh was subjected to shear forces. As expected, for both plate thicknesses a linear distribution of transverse displacements was obtained.

In the third analysis the mesh was subjected to an external twisting moment. In the thin plate analysis, constant curvatures were obtained in both plate directions, and the transverse displacements agreed with the analytical thin plate solution. In the thick plate analysis, a slight non-symmetry in the displacement response (the third digit) was obtained due to the unsymmetric representation of the transverse shear deformations. This non-symmetry is not observed if the shear deformations are suppressed (which corresponds to thin plate theory) by choosing a large value for the shear correction factor k [2, p. 236] (or when using rectangular elements in the mesh).

Finally, it should be noted that the patch test is of course passed for the three membrane stress states (τ_{11}, τ_{22} and τ_{12} constants).

4.1.b Cantilever linear analyses

A cantilever of unit width, thickness 0.1 and lengths 10 and 100 was subjected to a tip bending moment. The structure was modeled using one single element and two distorted elements as shown in Fig. 5. The results obtained in these analyses for the displacements and rotations at the cantilever tip and the stresses were those of Bernoulli beam theory.

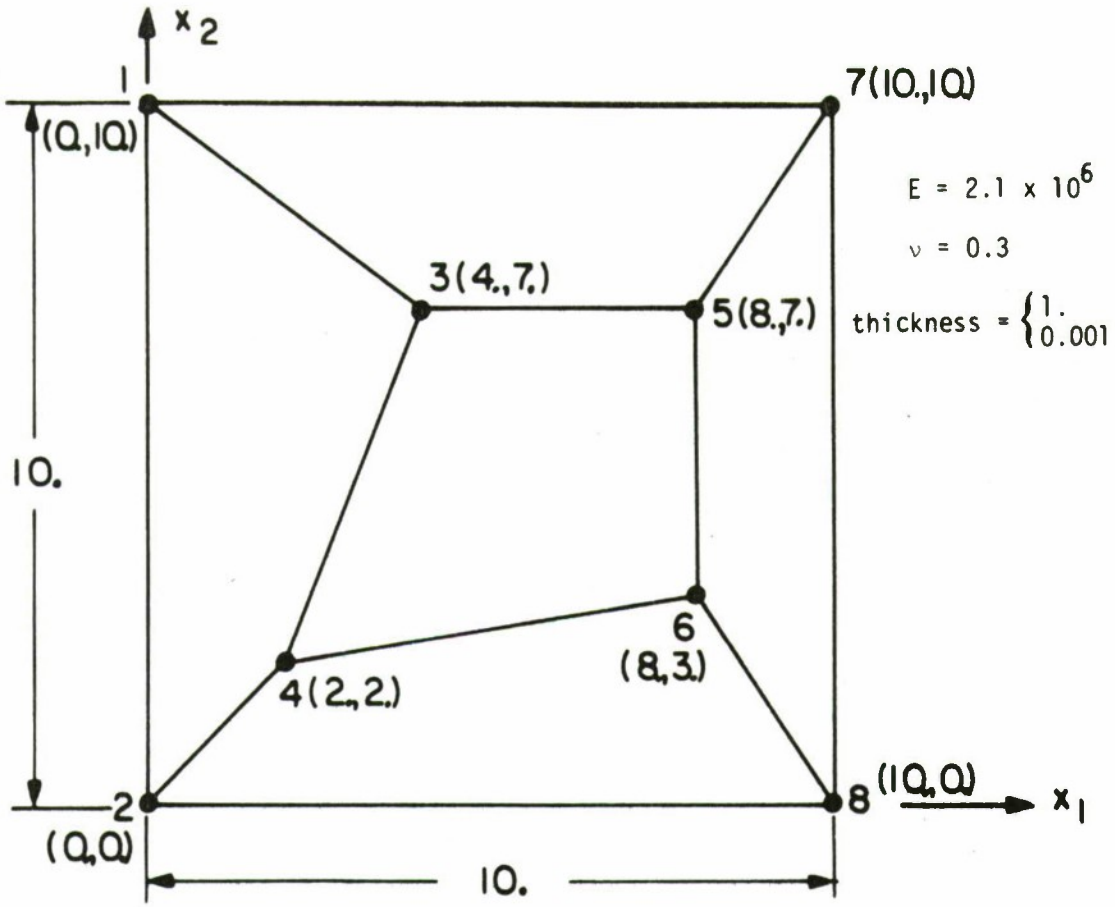

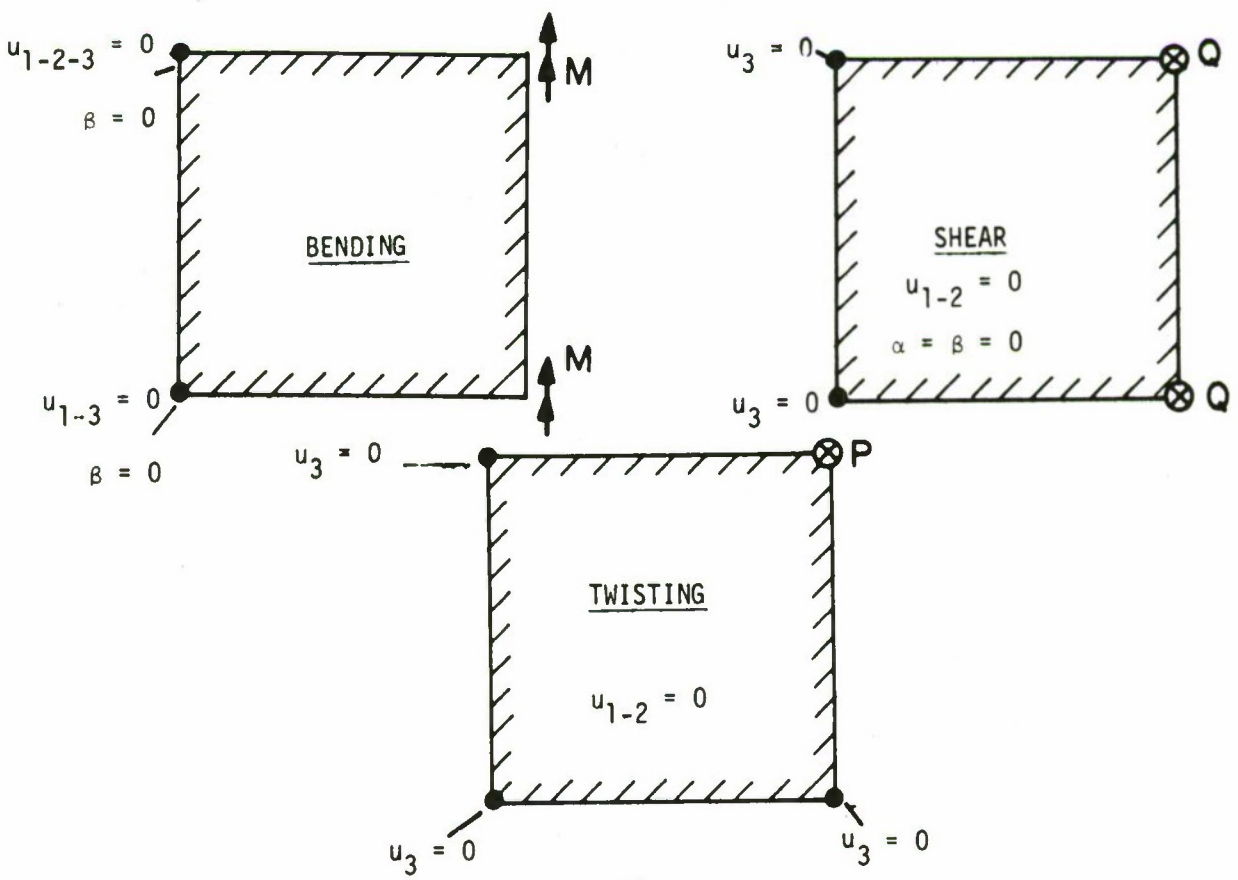

Figure 4 Patch tests

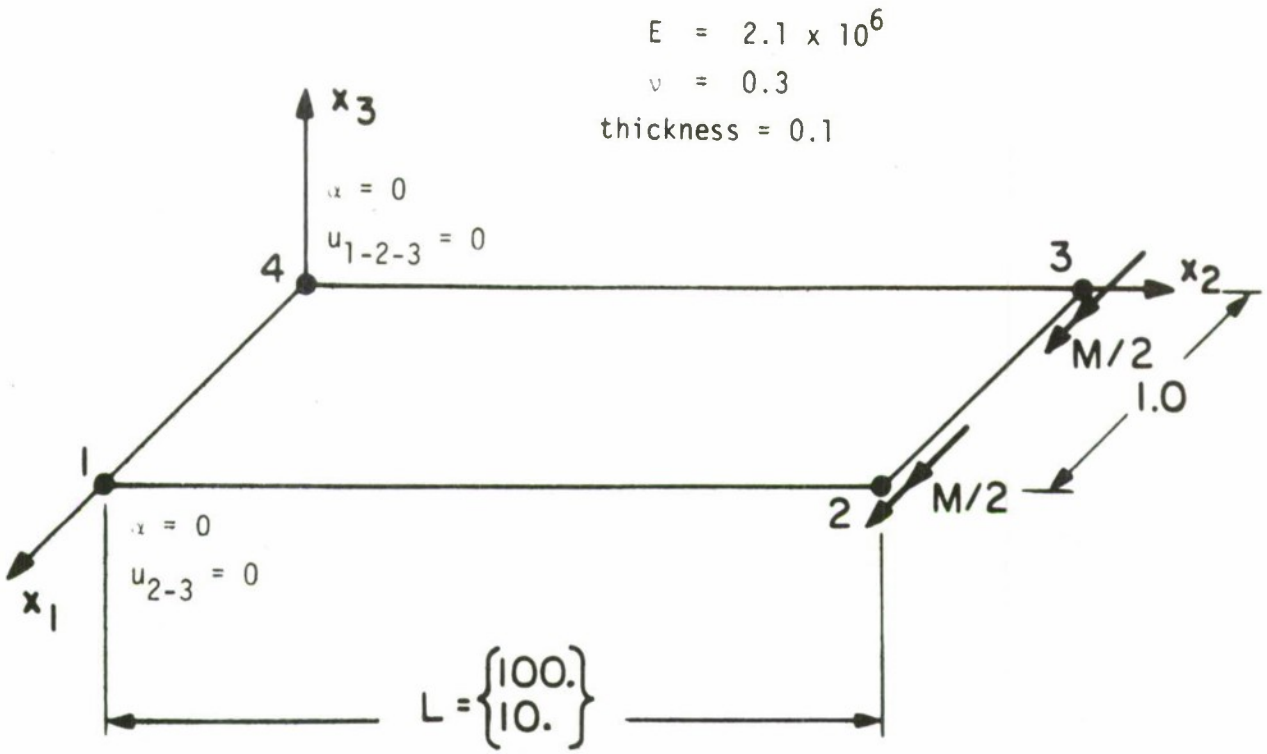

a) One element case

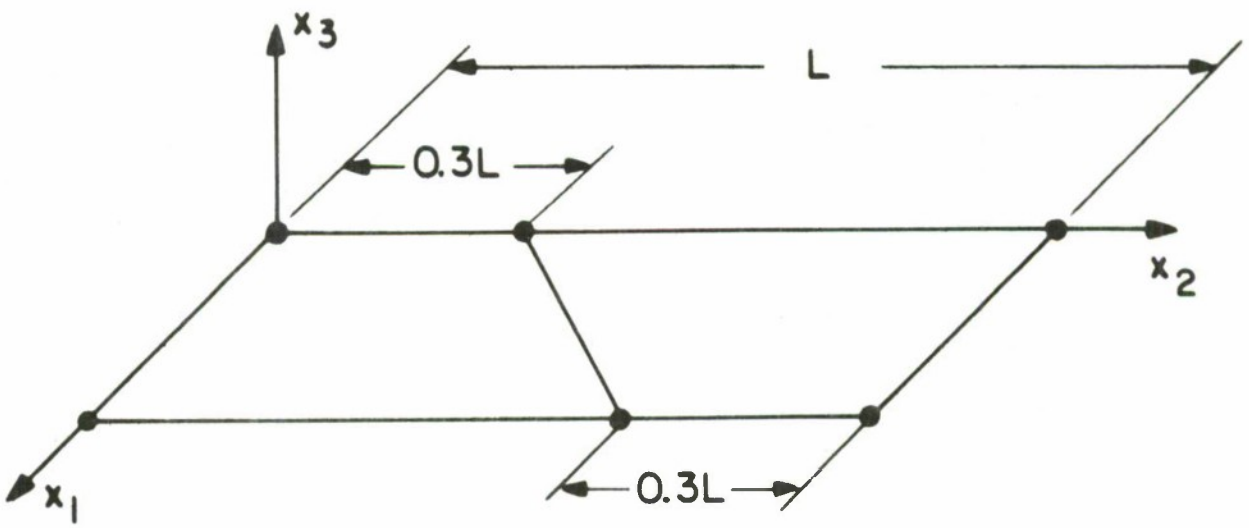

b) Two element case

Figure 5 Cantilever subjected to tip bending moment

Next, the cantilever in Fig. 6(a) was analyzed for the transverse tip load shown. Using 4 equal size elements to idealize the cantilever, again good results were obtained when compared with beam theoretical results.

Finally, the elements modeling the cantilever were distorted as shown in Fig. 6(b) for a thin and a thick cantilever. The results show that the transverse displacements and normal bending stresses are almost insensitive to the element distortions. However, the calculated transverse shear stresses (not shown in the figure) are not accurate.

4.1.c Linear analyses of a simply-supported plate

A simply-supported plate was considered for a static and a frequency analysis using a consistent mass matrix. To model one quarter of the plate a 4x4 mesh of equal elements was used. Figure 7 gives a comparison of the numerically and analytically predicted results. The same plate was also analyzed using the distorted element mesh also shown in Fig. 7(a) and the results of Fig. 7(c) were obtained.

4.1.d Analysis of a rhombic cantilever

The rhombic cantilever shown in Fig. 8, fixed at one side and subjected to constant pressure was analyzed using a 4x4 element mesh. The results for the transverse displacements at six locations are compared against the solutions obtained using the DKT triangular element of ref. [6], experimental measurements [1] and using the 16-node isoparametric element (with 4x4x2 Gauss integration). In all cases a one step geometric nonlinear analysis with equilibrium iterations was performed. Good correspondence between the experimental results and the solution obtained using our new 4-node element is observed.

4.2 Linear analysis of a cylindrical (Scordelis-Lo) shell

The shell structure shown in Fig. 9 has frequently been used to test the performance of shell elements [12]. Figure 9 shows the solutions obtained with our elements. In each of the solutions uniform meshes with equal sized elements were employed over one quarter of the shell. Solutions obtained using the 3-node DKT triangular element [25] and the 16-node isoparametric element [25] are also shown.

4.3 Linear analysis of a pinched cylinder

The pinched cylinder problem shown in Fig. 10 was also frequently analyzed to test shell elements. Figure 10 shows the convergence behaviour obtained with our new element, when comparing the finite element solutions with the solution given in refs. [11, 21]. Note that using the isoparametric shell element of ref. [3], also a fairly large number of degrees of freedom are required to predict the response of the cylinder accurately.

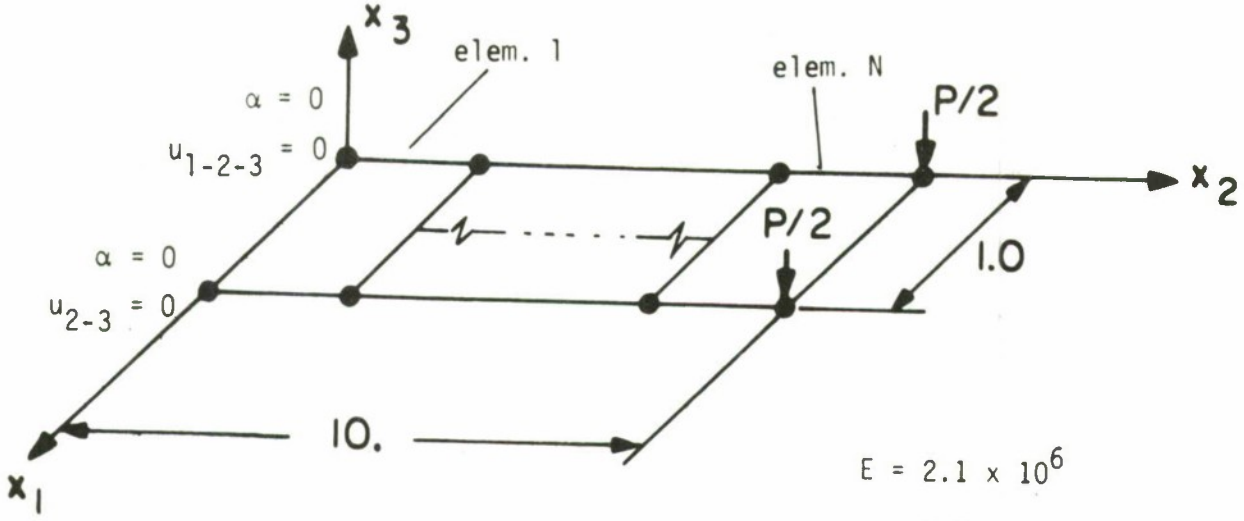

$E = 2.1 \times 10^6$

$\nu = 0.0$

thickness = 0.1

$P = 1.0$

N	$u_{3_{TIP}}^{FEM} / \left(\frac{PL^3}{3EI} + \frac{PL}{AG}\right)$
1	0.750
4	0.984

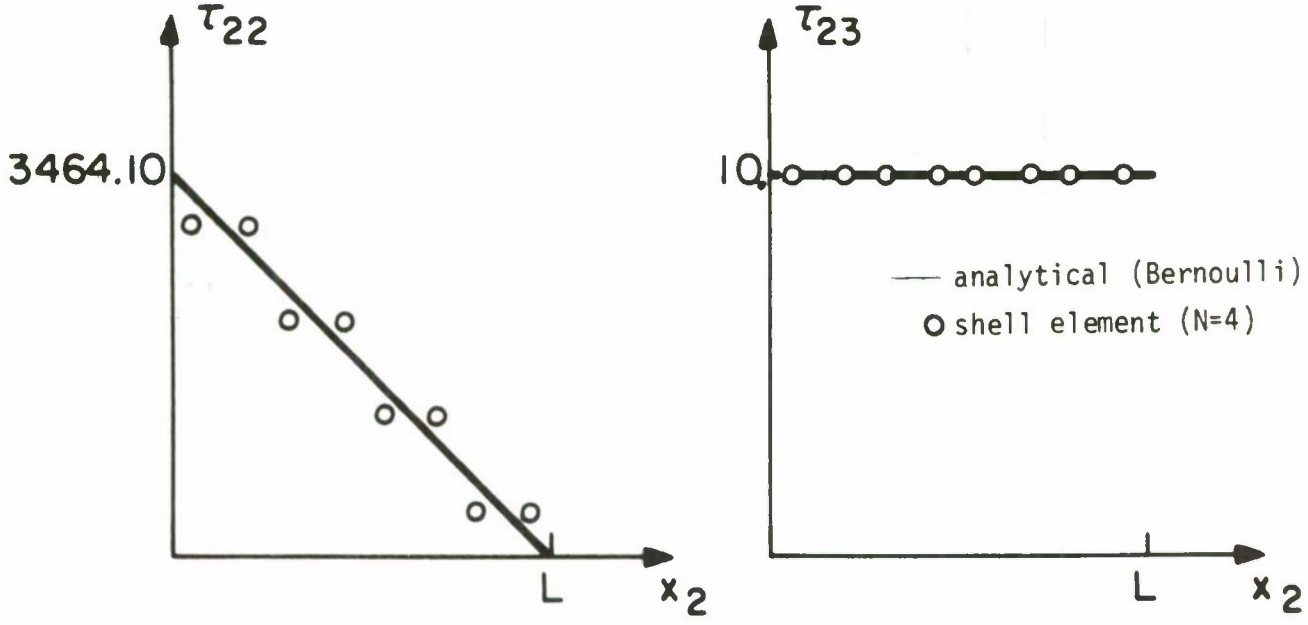

a) Solution using non-distorted elements

Figure 6 Response of a cantilever subjected to transverse tip load, stresses shown are those at the Gauss integration stations $r_3 = 0.57735$; τ_{pp}, is the principal stress in the distorted mesh, and its direction was always less than 11 degrees from the x_2 axis.

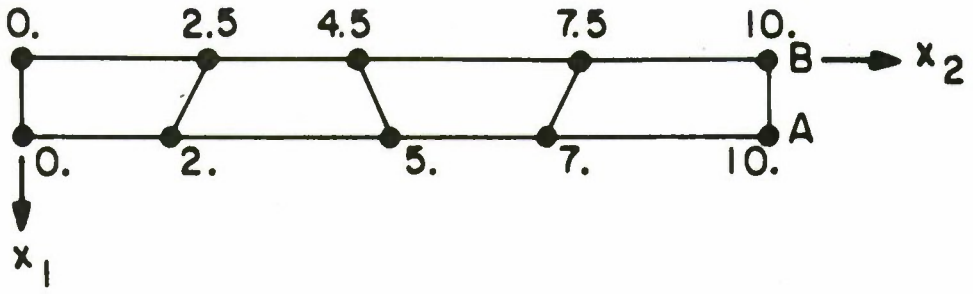

thickness	η|point B	η|point A
0.1	0.989	0.996
2.0	1.0013	0.9995

η = (u_3 distorted mesh)/(u_3 non-distorted mesh)

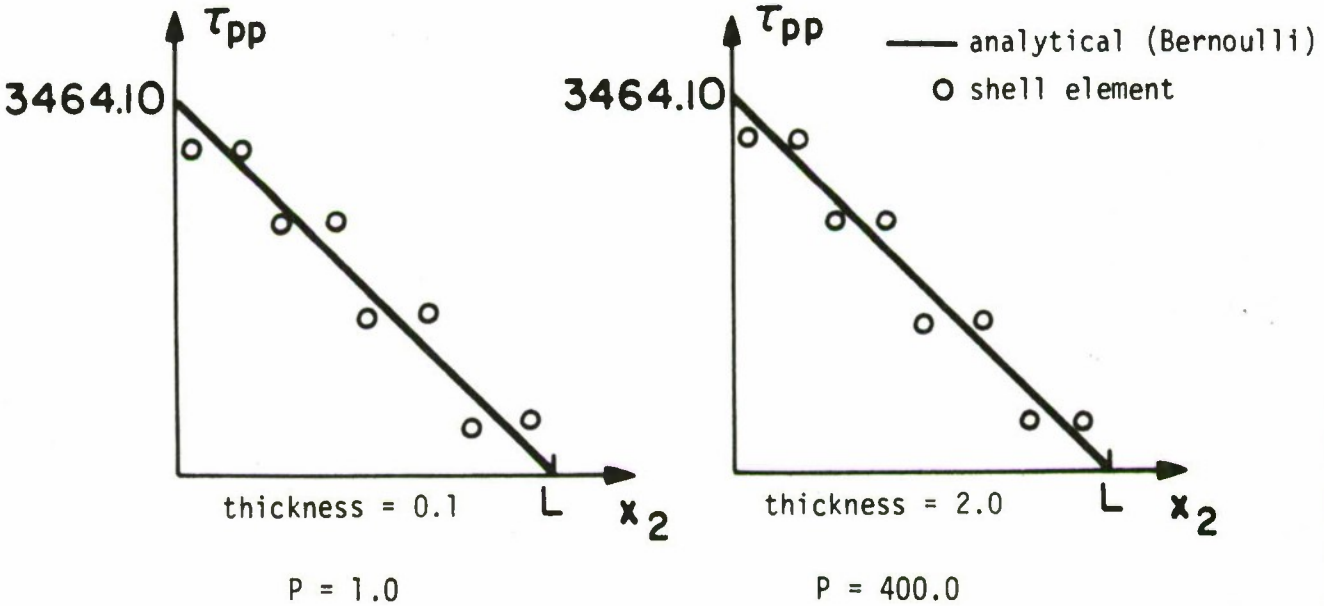

b) Solution using distorted elements

Figure 6 continued

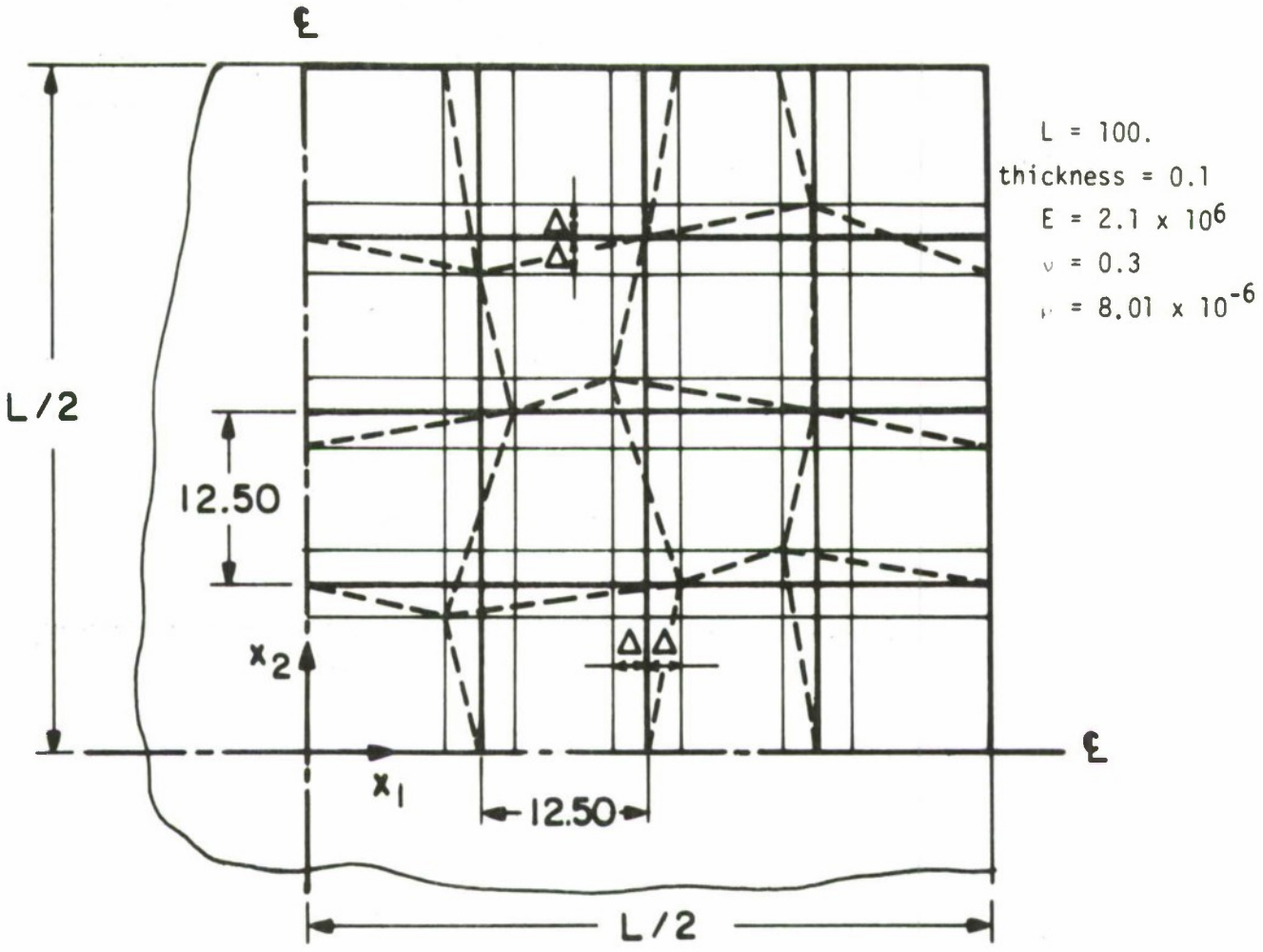

a) Finite element models

Mode shape	$f^{FEM} / f^{thin\ plate}$
1-1	1.02
1-3	1.18
3-3	1.17

b) Natural frequencies (cycles/sec) calculated using the non-distorted mesh

Figure 7 Linear analysis of a simply-supported square plate, the parameter of distortion, Δ, was equal to 2.50.

Model	$u_3^{FEM}/u_3^{thin\ plate}$ at center
non-dist.	0.995
dist.	0.992

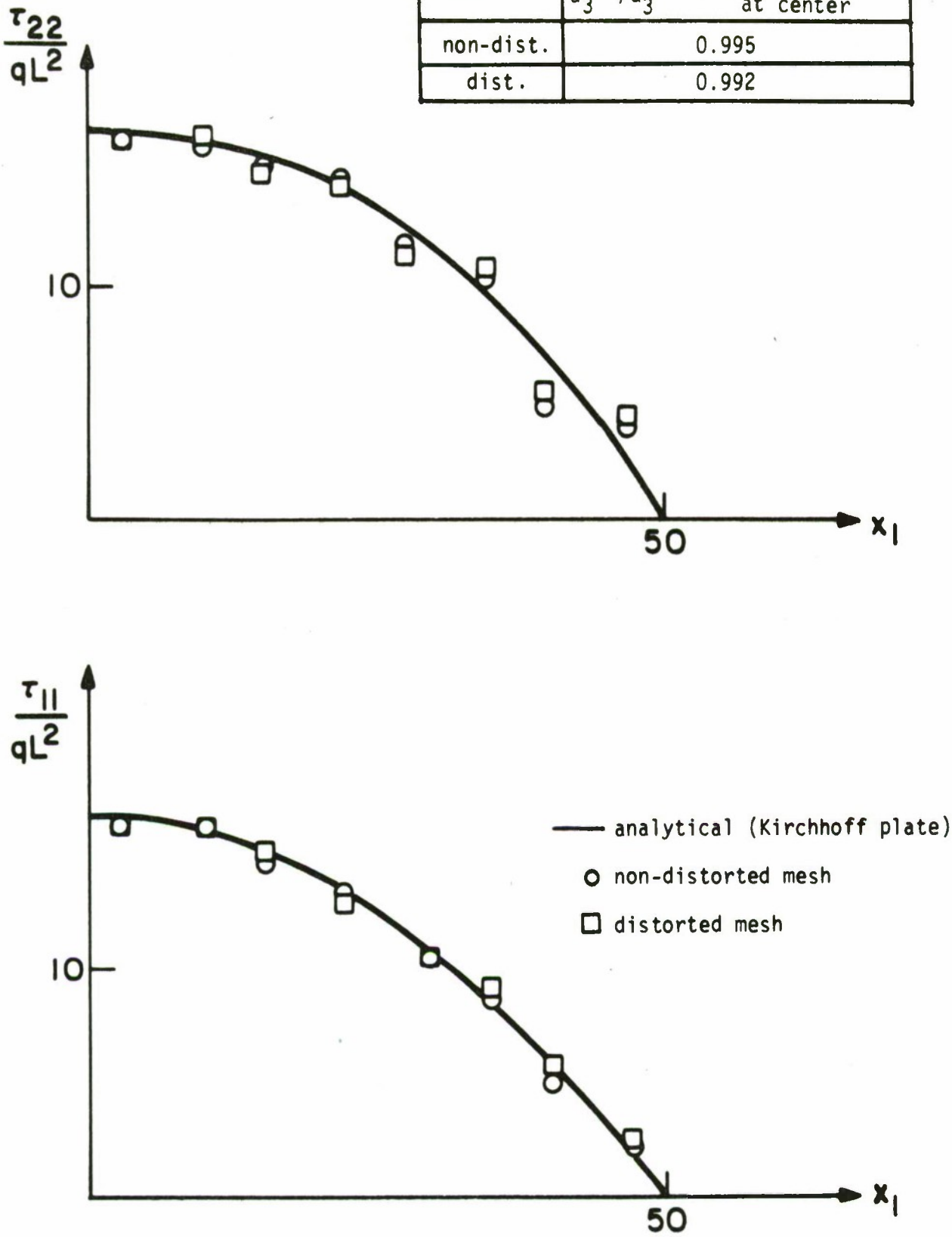

c) Static response due to constant pressure loading, stresses are given along line $x_2 = 0$, $x_3 = 0.028868$.

Figure 7 continued

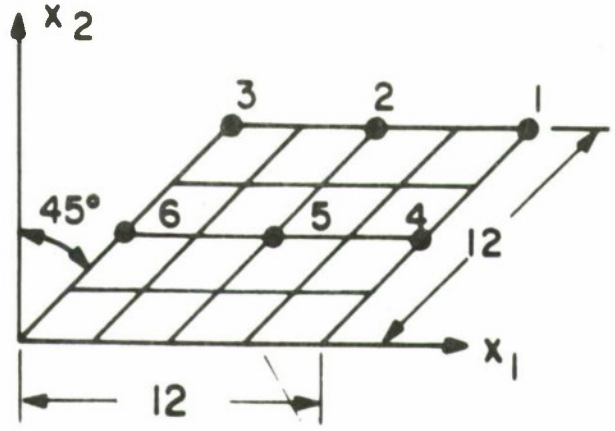

q = 0.26066

E = 10.5×10^6

thickness = 0.125

ν = 0.3

u_{1-2-3} = [illegible] = [illegible] = 0

4 x 4 mesh — 4-node elements

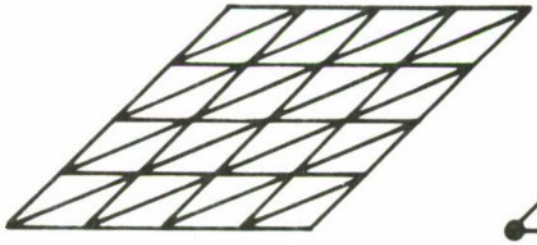

4 x 4 mesh — DKT elements

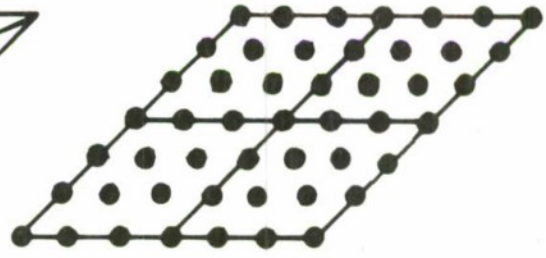

2 x 2 mesh — 16-node elements
(Int. 4x4x2)

Element	Mesh	CPU time / CPU time of DKT	Deflection at location					
			1	2	3	4	5	6
DKT	4x4	1.00	0.293	0.196	0.114	0.118	0.055	0.024
4-node	4x4	approx. 2	0.272	0.183	0.106	0.102	0.046	0.019
16-node	2x2	approx. $6\frac{1}{2}$	0.266	0.182	0.110	0.105	0.048	0.019
Experimental [1]			0.297	0.204	0.121	0.129	0.056	0.022

Figure 8 Response of rhombic cantilever subjected to constant pressure

R = 300.

L = 600.

ϕ = 40°

thickness = 3.0

E = 3. x 10^6 ν = 0.0

specific weight = 0.208333

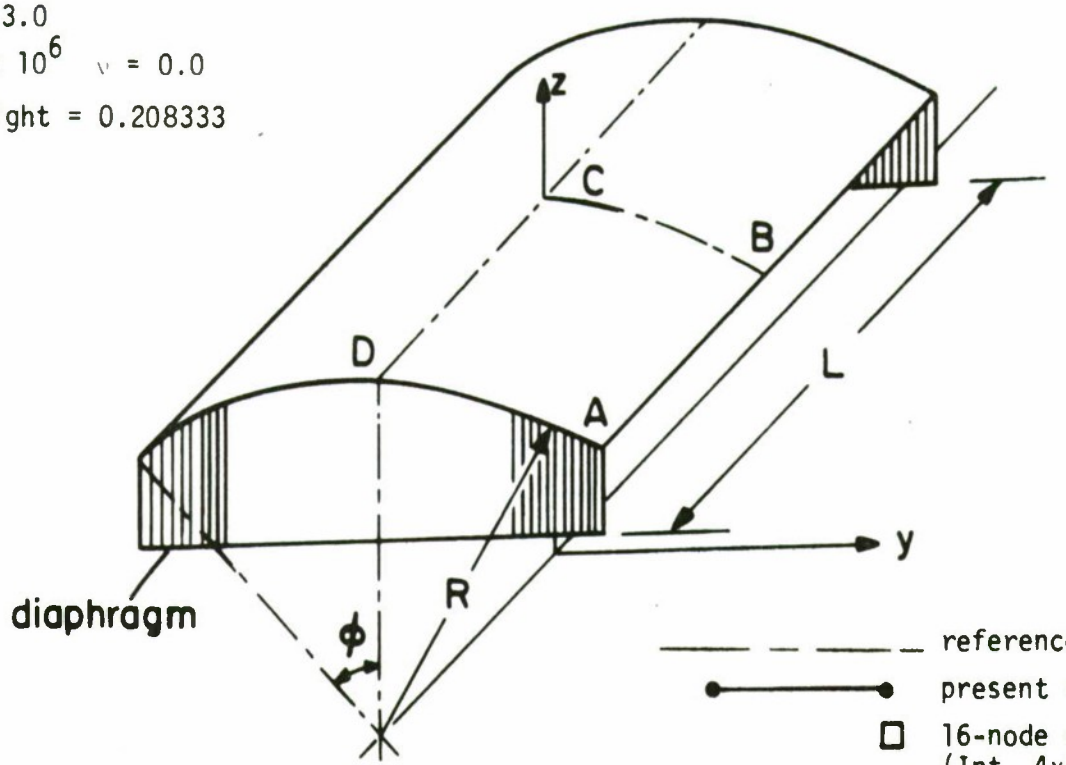

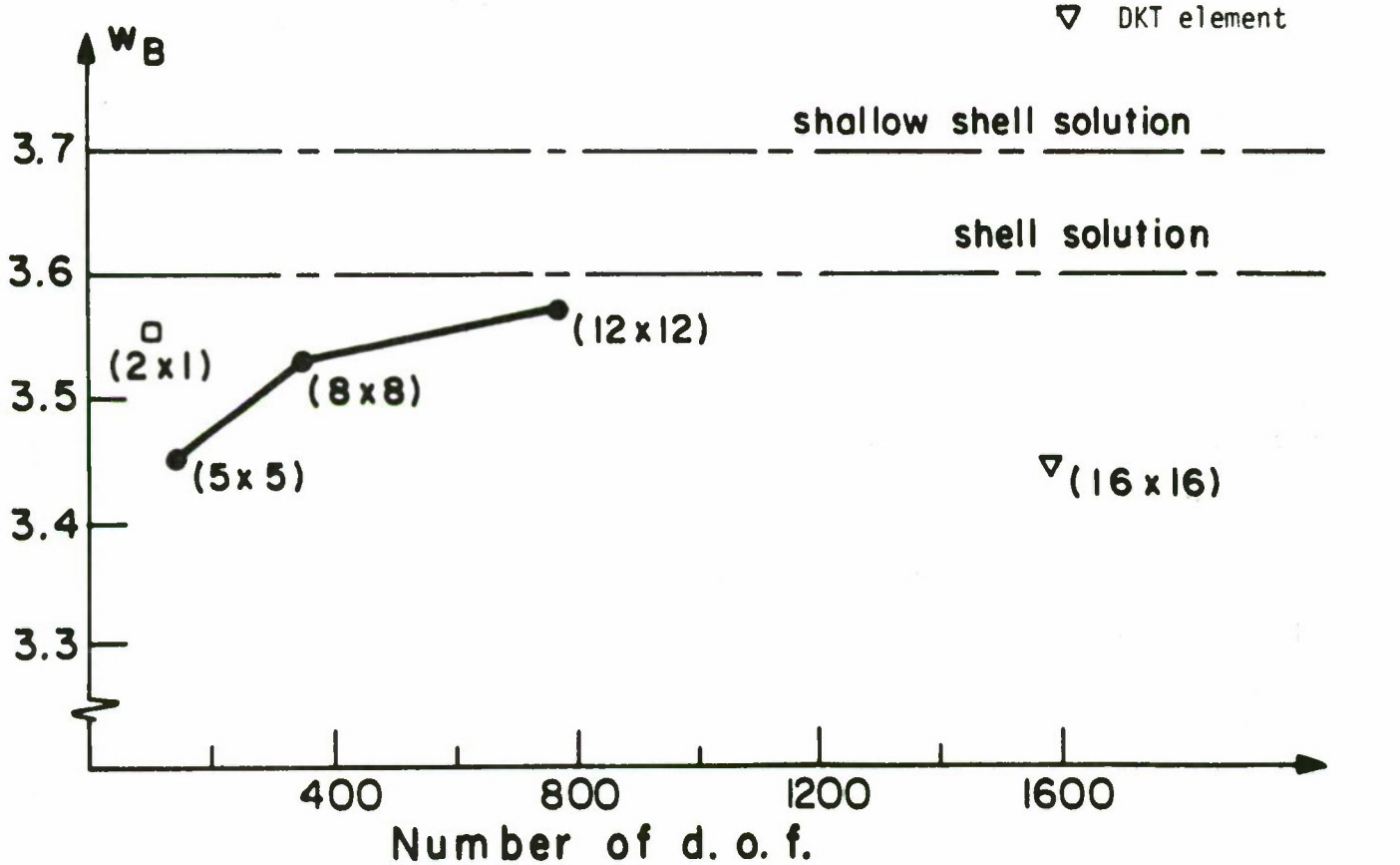

Figure 9 Linear analysis of a cylindrical shell subjected to dead weight. The 2x1 result refers to the solution obtained with two 16-node shell elements spanning from C to B. The 16x16 result refers to the use of 512 equal triangular DKT elements.

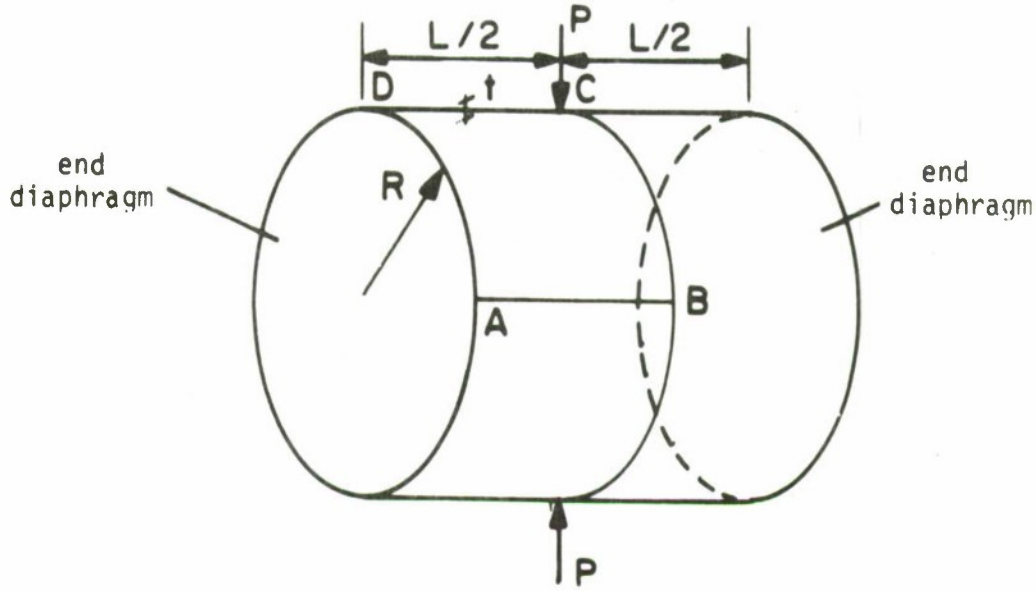

R/t = 100. $w_C = \frac{W_C E t}{P}$ w_C series solution =-164.24

L/R = 2. by Lindberg et. al.

Mesh for $\frac{1}{8}$th of shell	Number of d.o.f.	$\hat{w}_C^{FEM} / \hat{w}_C^{analyt.}$
5x5	130	0.51
10x10	510	0.83
20x20	2020	0.96

a) Convergence study for 4-node element

Element	Mesh for $\frac{1}{8}$th of shell	Number of d.o.f.	$\hat{w}_C^{FEM} / \hat{w}_C^{analyt.}$
4-node	20x20	2020	0.96
16-node	10x10	4530	0.98

b) Comparison between 4-node and 16-node elements

Figure 10 Linear analysis of a pinched cylinder; u = axial displacement, w = radial displacement

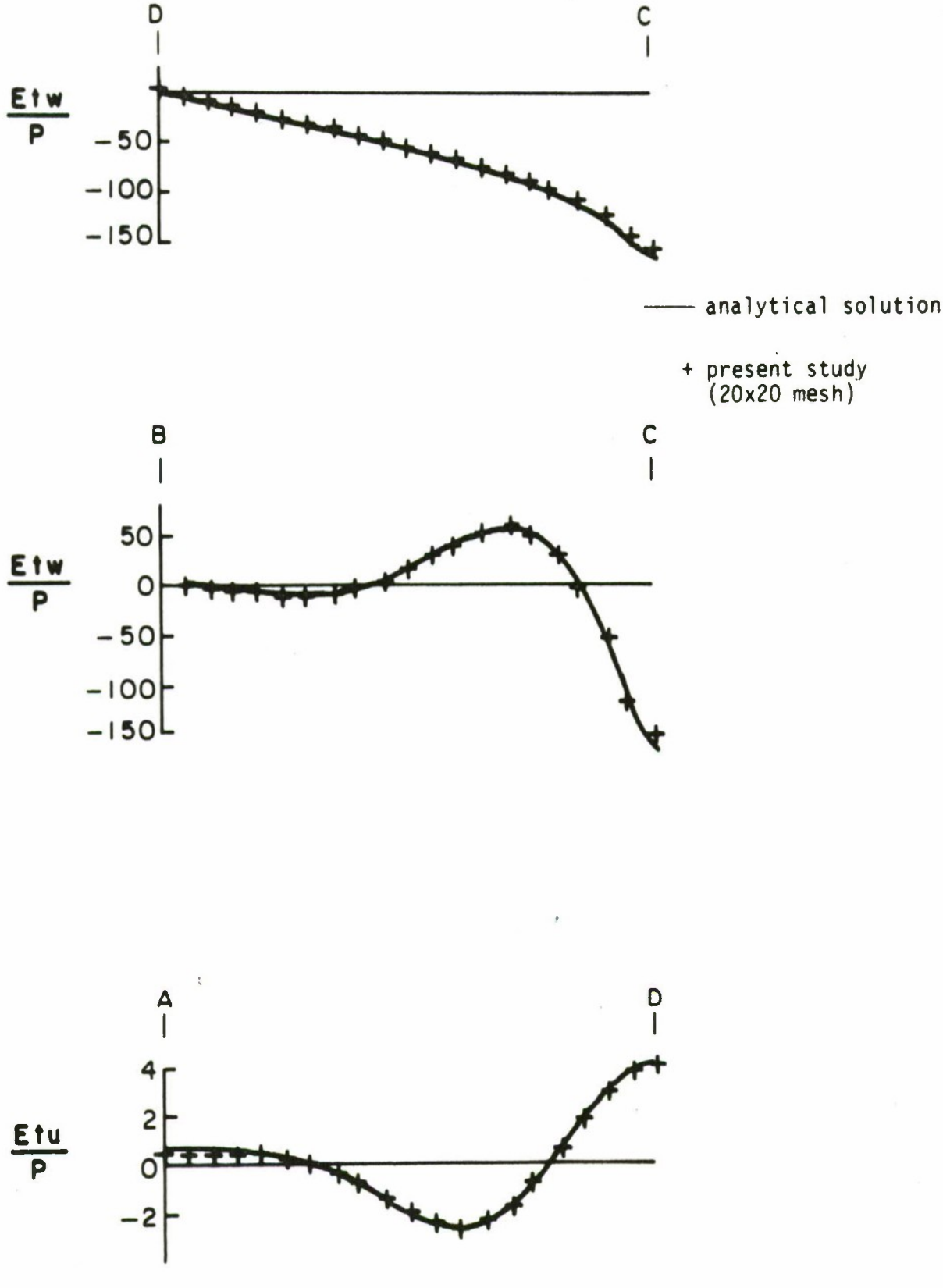

c) Displacements

Figure 10 continued

4.4 Large deflection analysis of a cantilever

The cantilever shown in Fig. 11 was analyzed for its large displacement and large rotation response. This is a typical problem considered to test the geometric nonlinear behaviour of beam and shell elements [25]. Figure 11 shows also the models used in the analysis.

The first two models are single element, cubic and parabolic isoparametric degenerate shell element models. Model I predicts the response of the cantilever very accurately, whereas model II yields an accurate response solution in linear analysis but locks once the element is curved in the nonlinear response solution. This observation is in accordance with the results reported in ref. [5].

The same nodal point layouts were next employed for models III and IV using our new 4-node shell element. Figure 11 gives also the results obtained with these models. It is seen that model III yields an accurate large displacement response prediction, and even model IV yields quite accurate results up to about 60 degrees of rotation. The computer time required in these analyses were only different using models I, III and IV.

Another important result is shown in Fig. 12. As reported in ref. [5], the cubic shell element is sensitive to "in-plane" distortions; and hence, it is interesting to study the effect of using a distorted element mesh in the analysis of the cantilever. Figure 12 summarizes the results obtained using the one cubic element and three 4-node elements with a nodal layout that corresponds to distorting the elements. It is seen that the predictive capability of our new 4-node element is considerably less sensitive to the element distortions.

4.5 Geometric nonlinear response of a shallow spherical shell

Figure 13 shows the spherical shell that was also analyzed in ref. [3] with one cubic shell element, modeling one quarter of the shell. To test our new 4-node shell element, the same nodal point layout as in ref. [3] was used, giving a mesh of nine elements. Figure 13 shows the response calculated, including the post-buckling response (not reported in ref. [3]) with the automatic load stepping algorithm of ref. [4]. Good correspondence with the analytical solution of Leicester [20] and the solution of Horrigmoe [16] was obtained. The solution with the 16-node element was almost twice as expensive as the 4-node element solution (using in both cases the same parameters for the automatic step-by-step solution algorithm).

4.6 Linear buckling analysis and large deflection response of a simply-supported stiffened plate

The stiffened plate shown in Fig. 14 was analyzed for its buckling response. Since we expect the buckling mode to be symmetric [26] only one

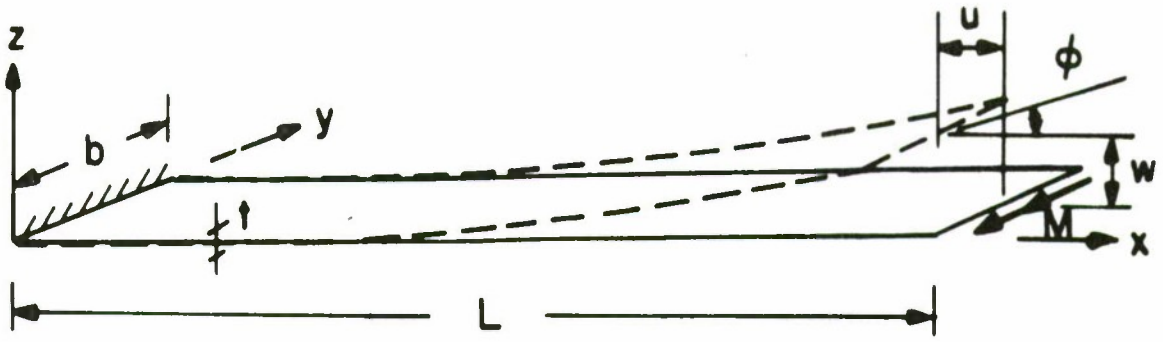

b = 1.0 E = 1800.

t = 1.0 ν = 0.0

L = 12.0

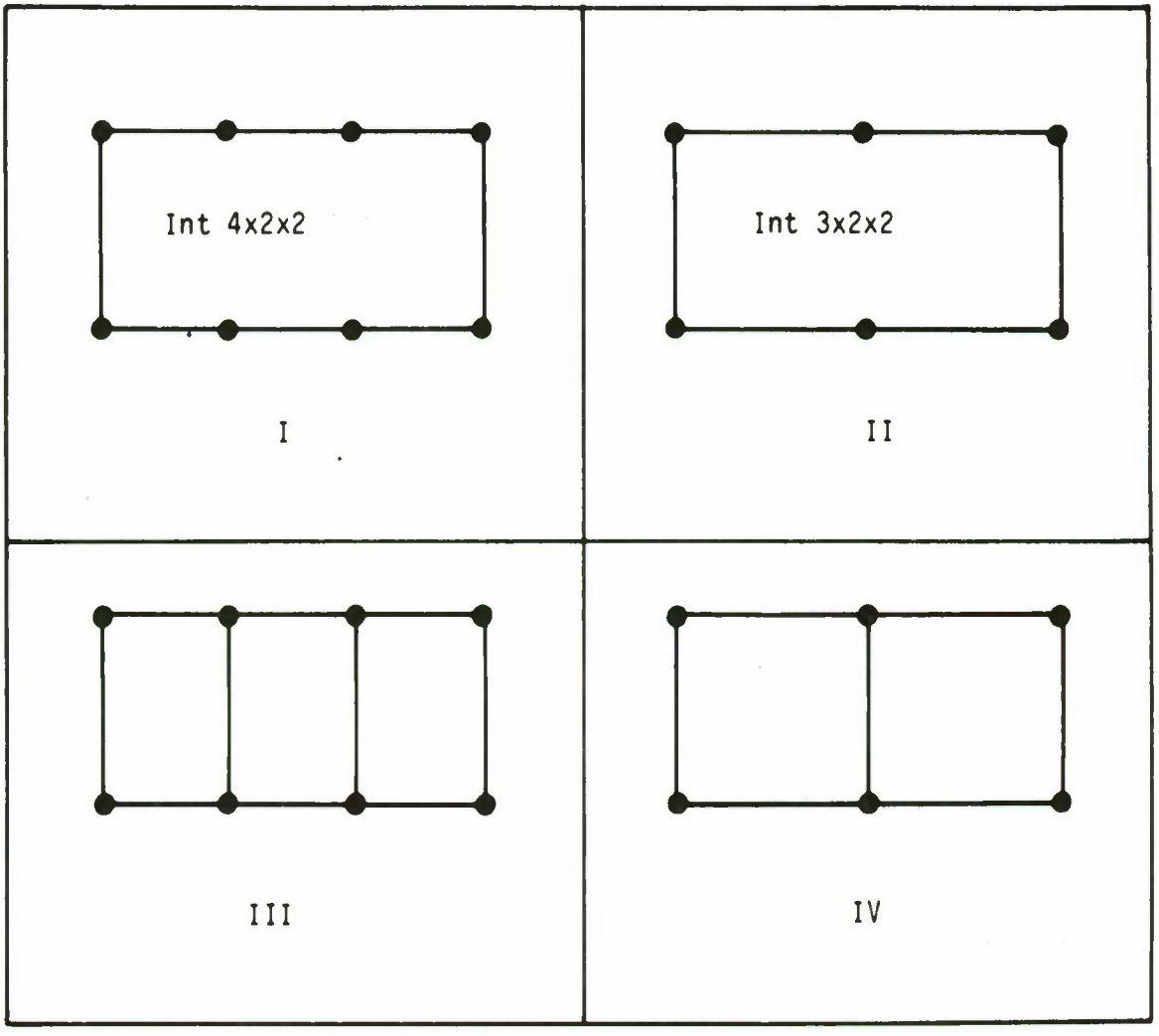

a) Finite element models

Figure 11 Large deflection analysis of a cantilever using non-distorted elements

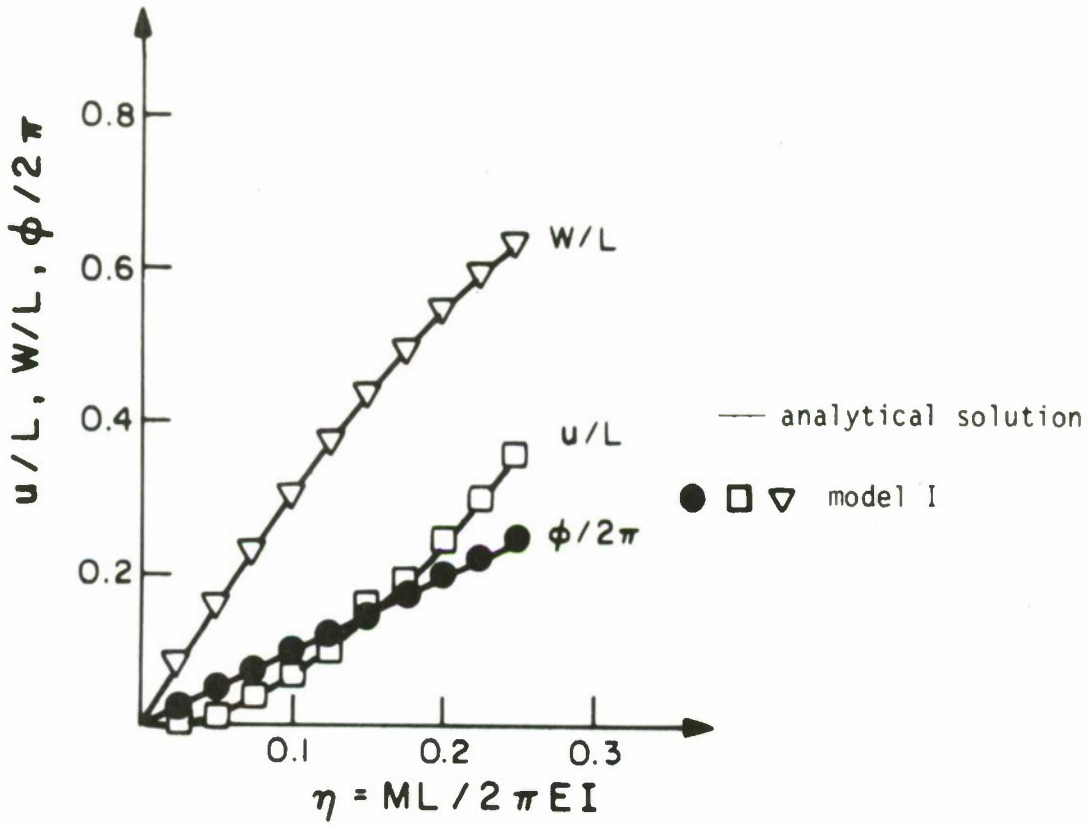

b) Response of model I

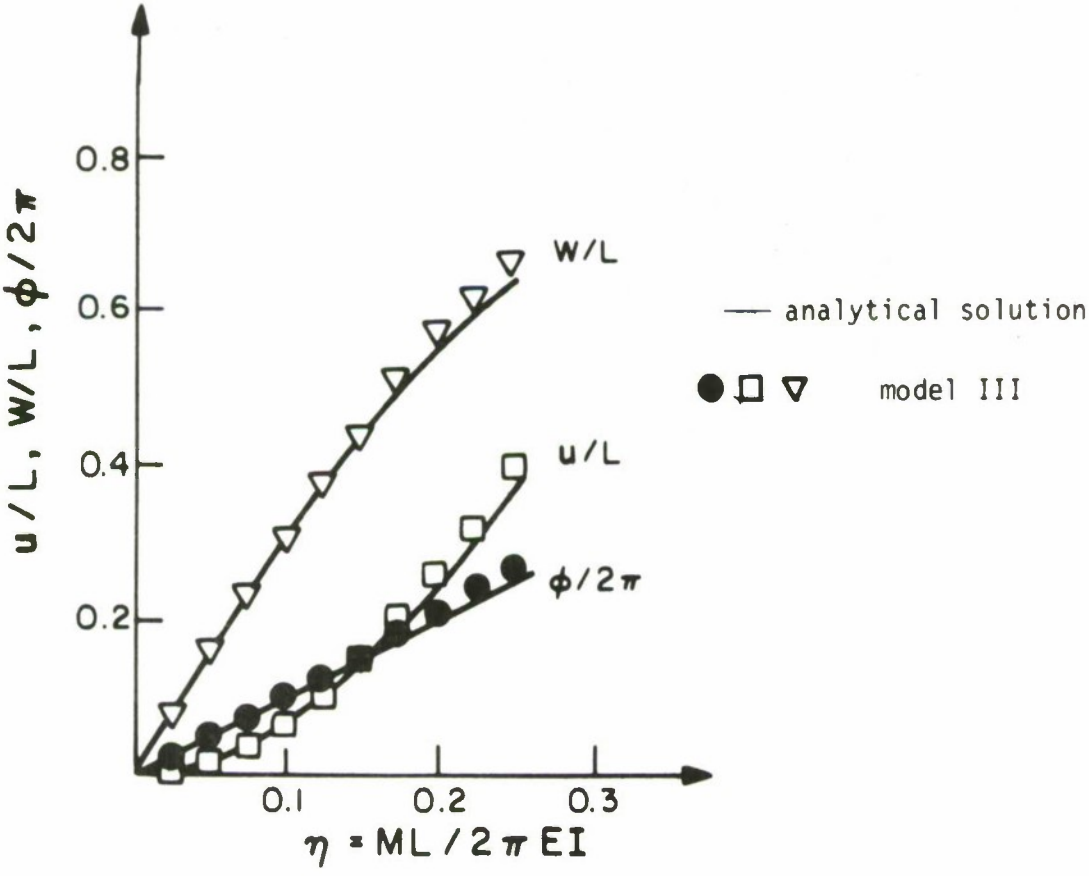

c) Response of model III

Figure 11 continued

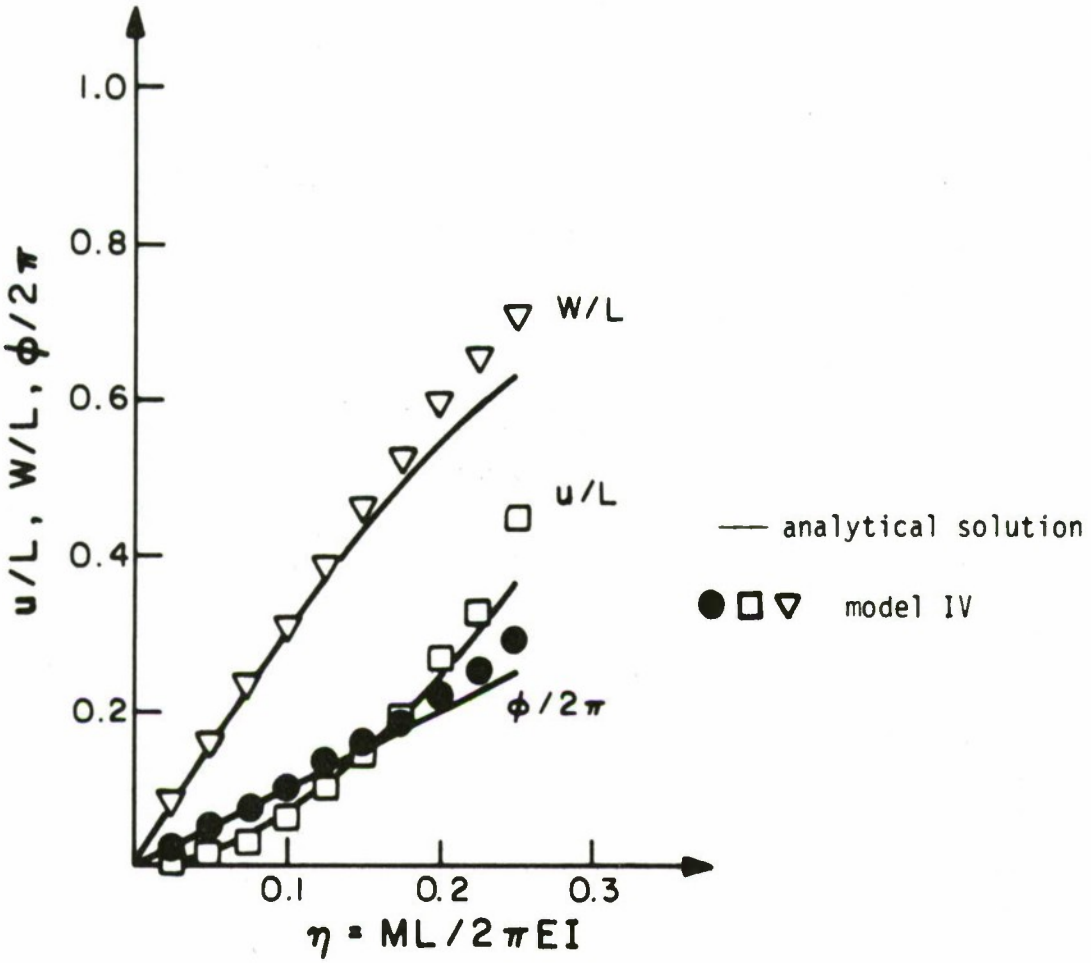

d) Response of model IV

Figure 11 continued

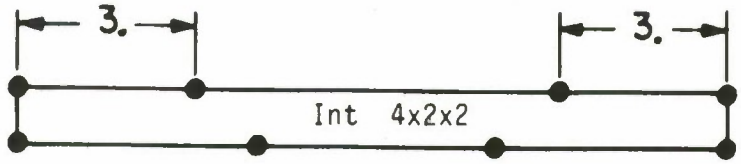

Model I - distorted

Model III - distorted

	Model I - distorted			Model III - distorted		
	step 2	step 5	step 8	step 2	step 5	step 8
$\phi^{FEM}/\phi^{ANALYT.}$	0.13	0.13	0.13	0.95	0.84	0.76
$u^{FEM}/u^{ANALYT.}$	0.01	0.01	0.01	0.89	0.68	0.56
$w^{FEM}/w^{ANALYT.}$	0.10	0.11	0.12	0.95	0.86	0.81
$\phi^{ANALYT.}$	18°	45°	72°	18°	45°	72°

Figure 12 Large deflection analysis of a cantilever using distorted elements

$R_1 = R_2 = 2540.$

$a = 784.90$

$h = 99.45$

$E = 68.95$

$\nu = 0.3$

All edges are hinged and immovable.

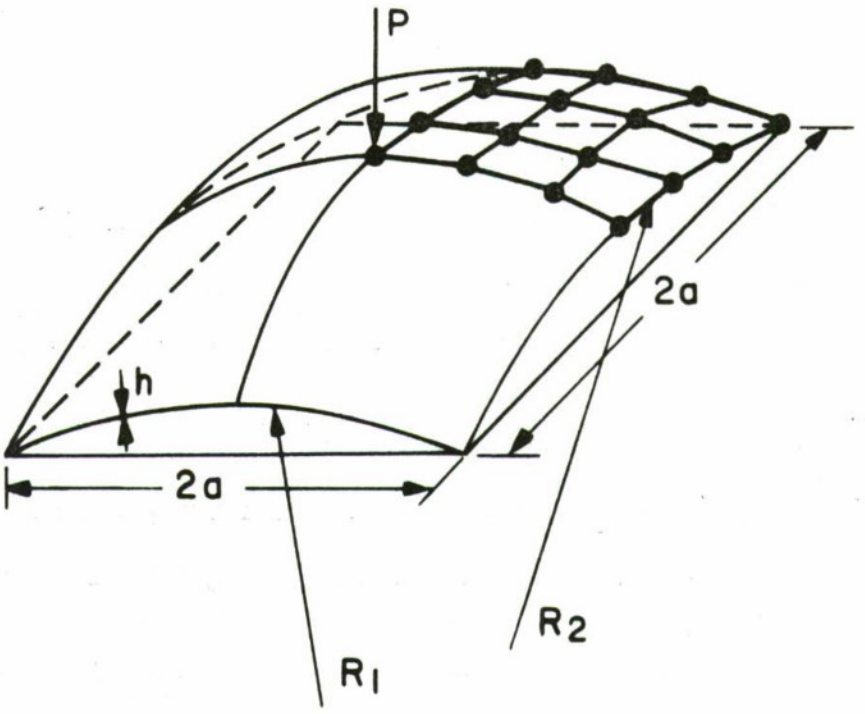

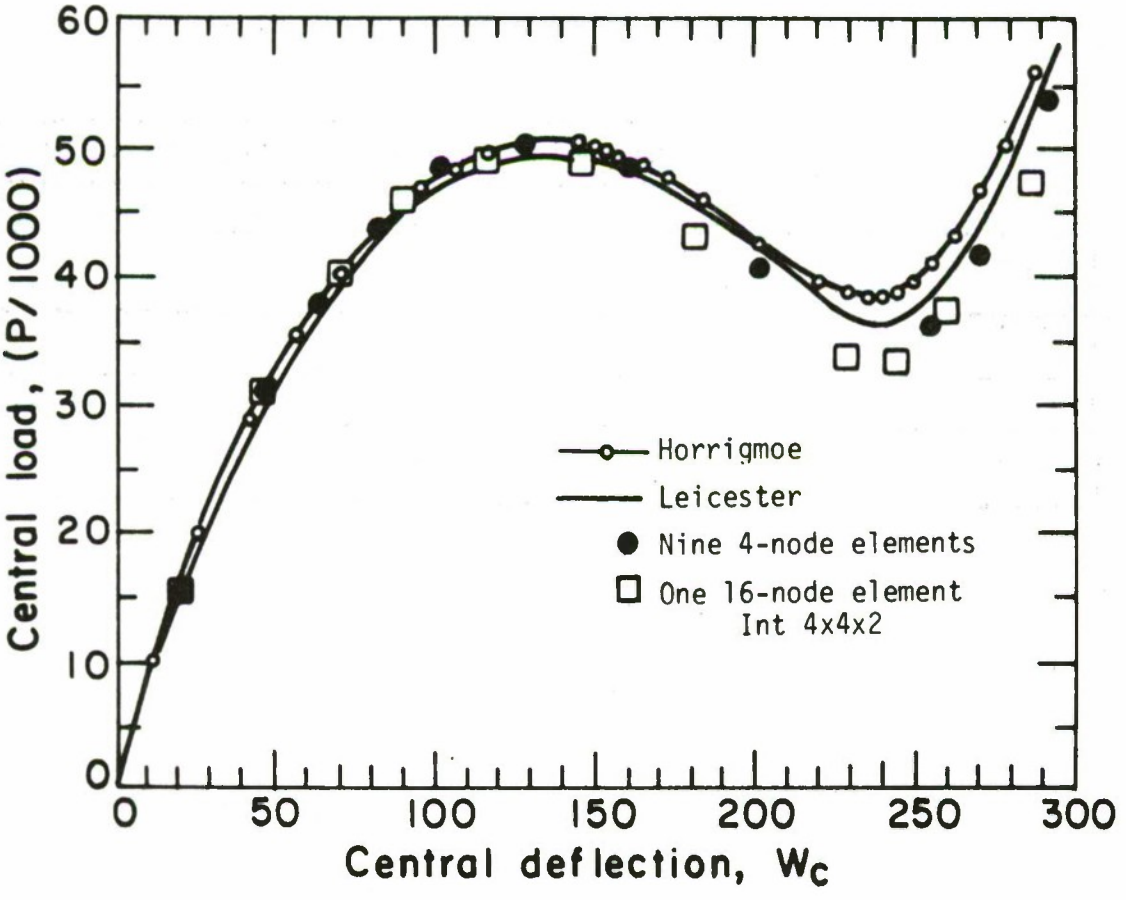

Figure 13 Geometric nonlinear response of a spherical shell

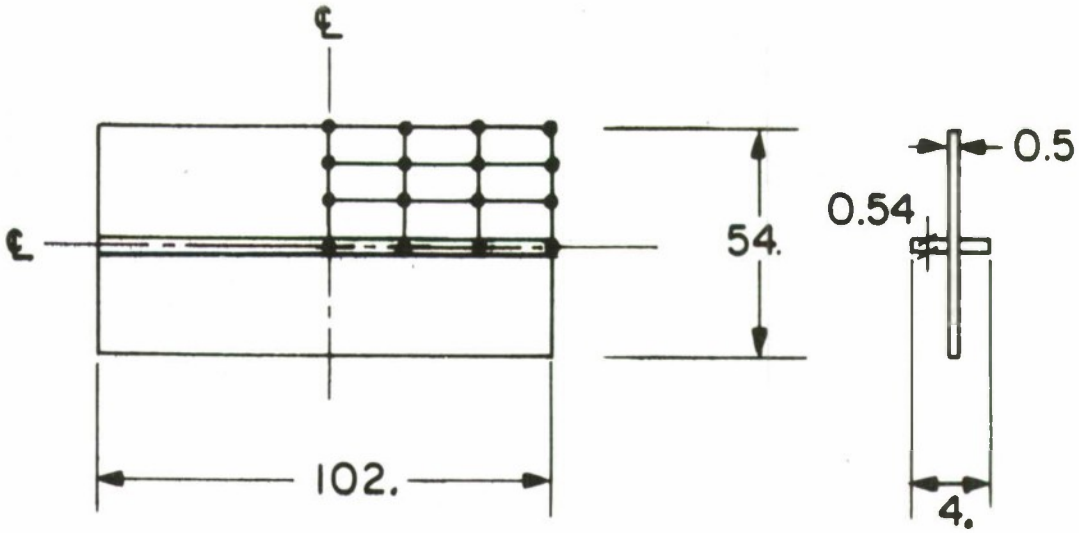

simply supported plate

$E = 2.1 \times 10^6$

$\nu = 0.3$

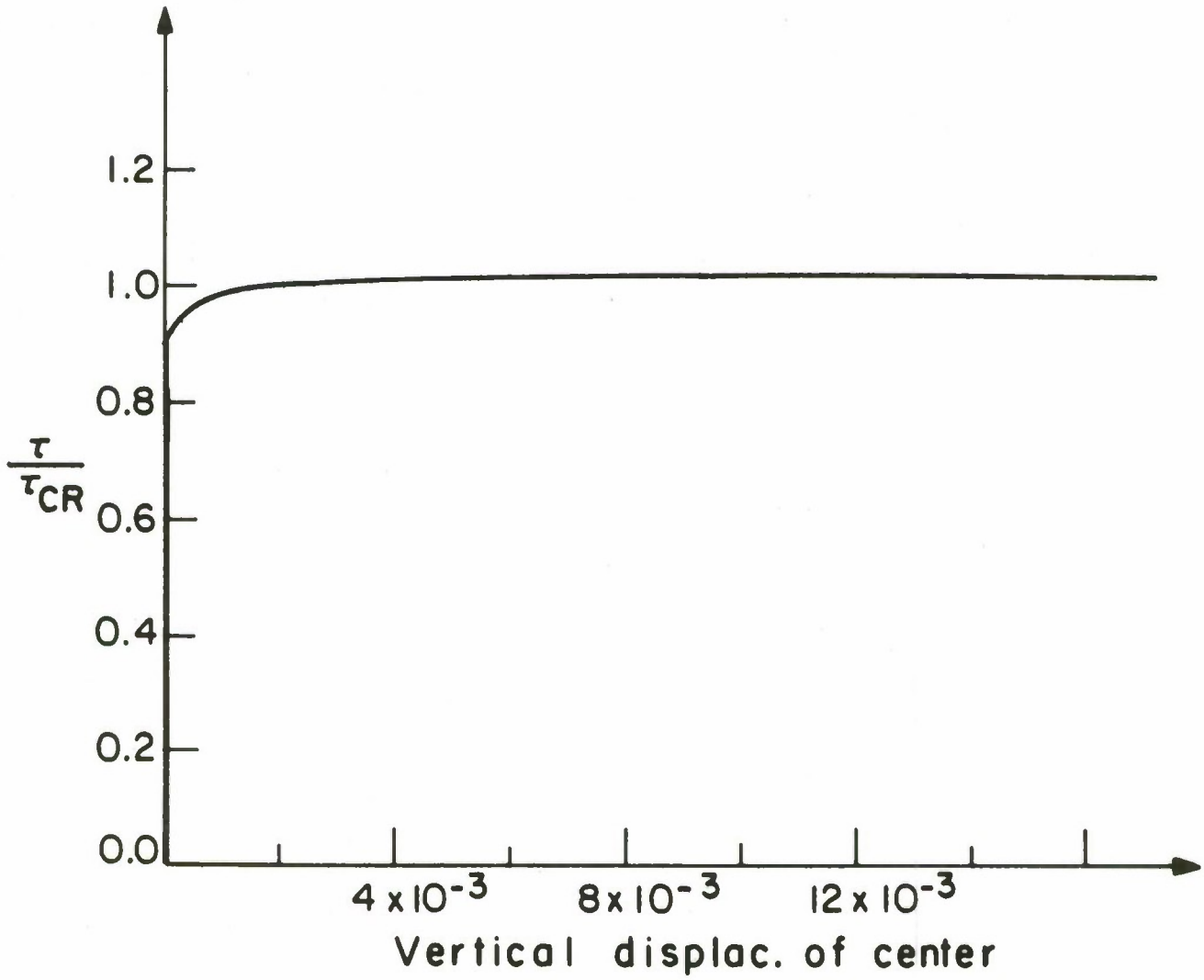

Figure 14 Nonlinear response of a stiffened plate

quarter of the plate is modeled using symmetry boundary conditions. The model consists of nine 4-node shell elements and three 2-node isoparametric beam elements. At the nodes where a shell element connects to a beam element, three rotational degrees of freedom aligned with the global axes are considered for the shell element. In order to avoid locking of the isoparametric beam elements, one point Gauss integration along the beam axes was used. This does not introduce spurious zero energy modes in the model, although the bending stiffness of the beam is under-estimated.

The linearized buckling problem was solved as described in [4, Eq. (37)] and we obtained

$$\frac{\sigma_{cr}\ (\text{finite element solution})}{\sigma_{cr}\ (\text{analytical solution})} = 1.02 \ .$$

Next, an initial imperfection with the shape of the first buckling mode and a maximum amplitude of 1/5th of the plate thickness was introduced. Figure 14 shows the large deflection response of this model as calculated using the automatic load stepping scheme of ref. [4] with a tight energy convergence tolerance.

4.7 Analysis of elasto-plastic response of a circular plate

The thin circular plate shown in Fig. 15 was analyzed for its elasto-plastic response, when subjected to a concentrated load at its center. The plate is simply-supported with its edges restrained from moving in its plane.

In a first solution, the plate model shown in Fig. 15(a) was used to analyze the plate assuming small displacements (materially-nonlinear-only conditions). Figure 15 shows that the theoretical collapse load is over-estimated, but for the coarse mesh used, the predicted response is quite reasonable.

In a second solution, large displacements and elasto-plastic conditions were assumed and in this case the stiffening behaviour of the plate shown in Fig. 15(b) was predicted. In order to have a comparison, also the model of five axisymmetric 8-node elements shown in Fig. 15(a) was solved. Figure 15 shows that both models predict in essence the same response; however, in this case relatively little plasticity was developed for the range of displacements considered.

4.8 Dynamic analysis of an elastic-perfectly plastic, simply-supported square plate

One quarter of the plate shown in Fig. 16 was modeled using sixteen 4-node elements. The central difference method was used in the time

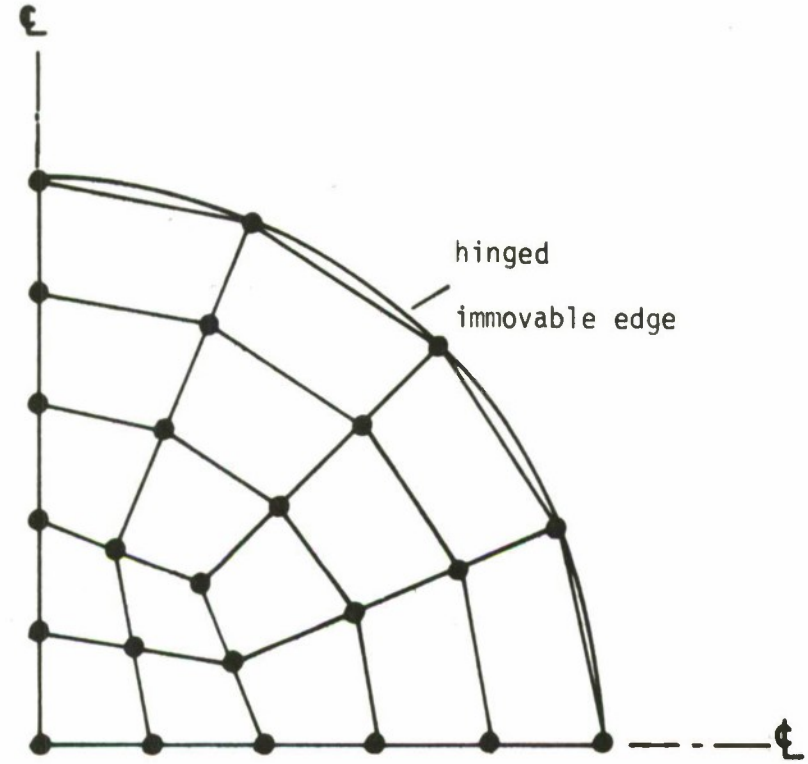

$R = 100$

$t = 1$

$E = 2.1 \times 10^6$ $E_T = 0.0$

$\nu = 0.3$

$\sigma_y = 1000$

4-node shell model

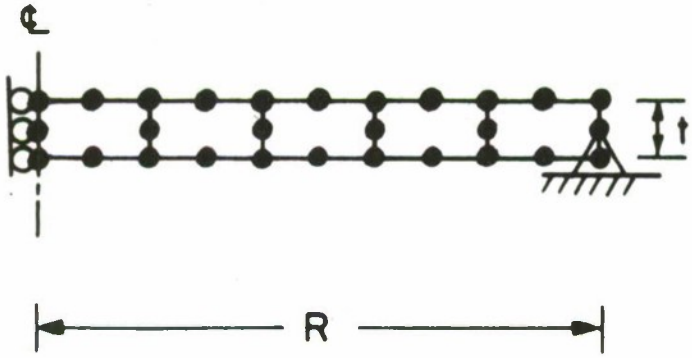

axisymmetric model

a) Finite element models

Figure 15 Response of elastic-perfectly plastic circular plate subjected to a concentrated load, P, at its center. TLF abbreviates use of total Lagrangian formulation and MNO abbreviates use of materially-nonlinear-only formulation.

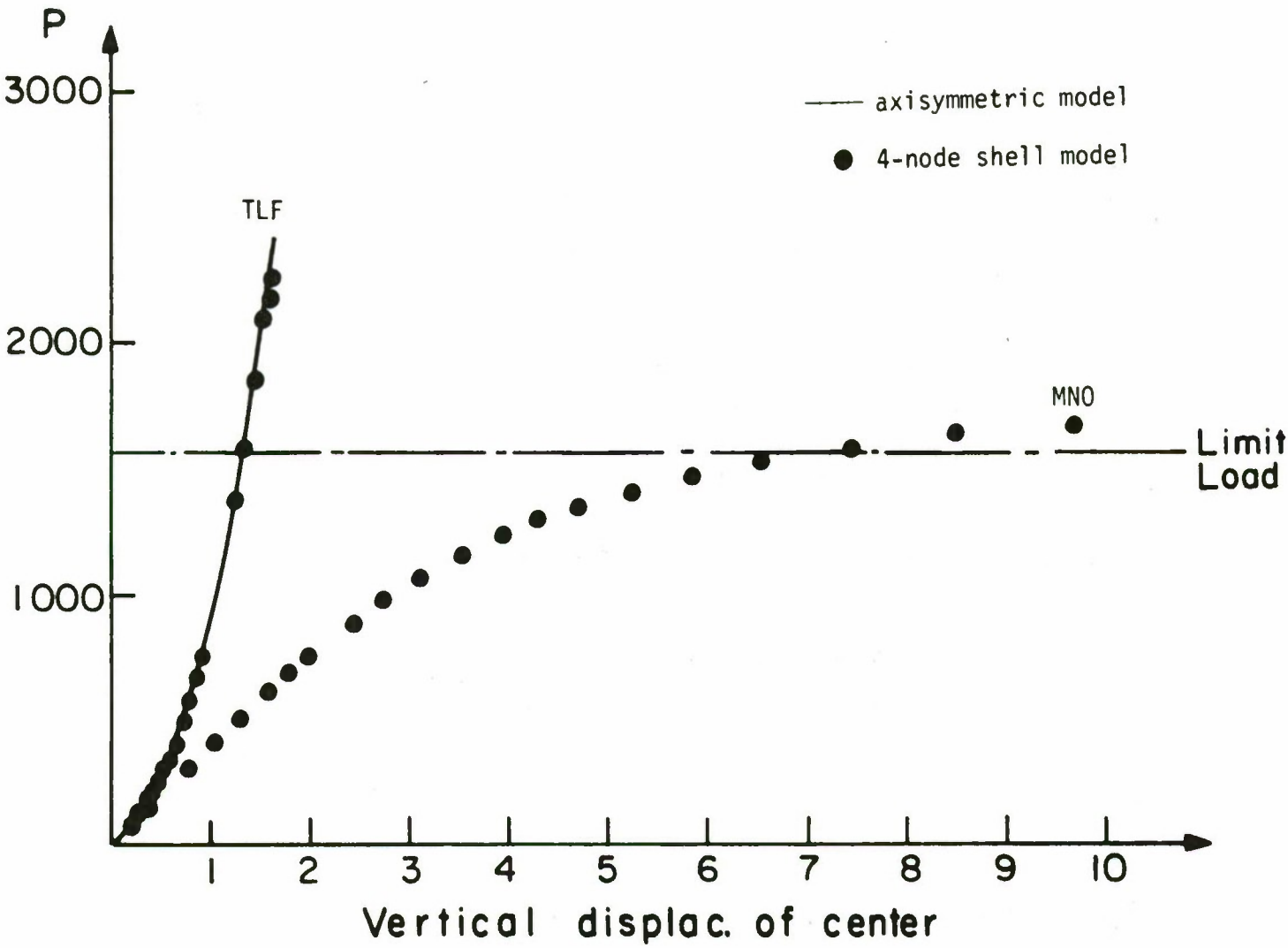

b) Circular plate response

Figure 15 continued

a = 10.

thickness = 0.5

$E = 10^7$ $\rho = 2.588 \times 10^{-4}$

$\nu = 0.3$ $\sigma_y = 30000.$

$E_T = 0.0$

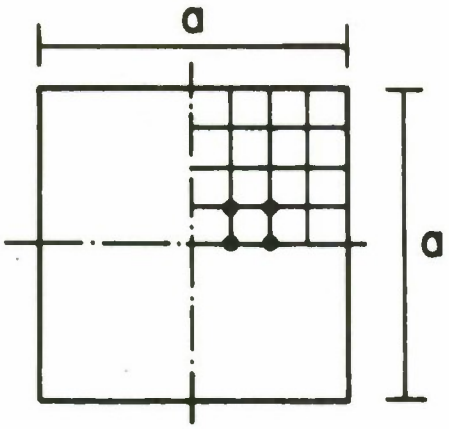

(a) Plate model

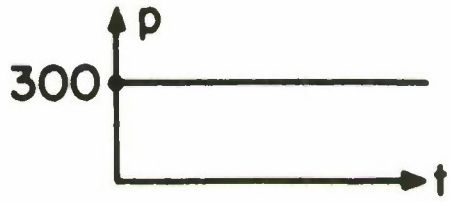

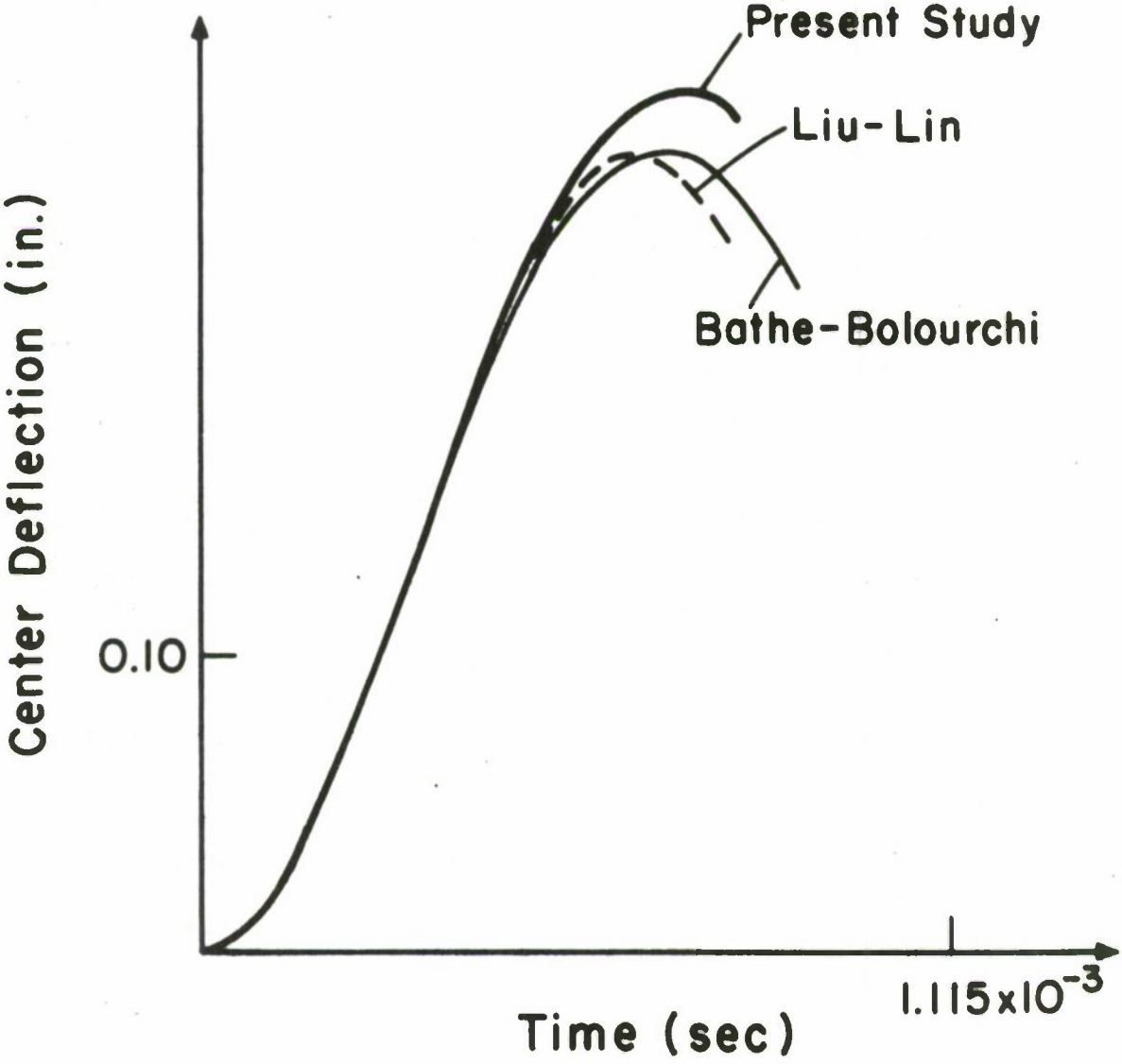

b) Time history

Fig. 16 - Dynamic Analysis of Elastic-Plastic Plate

integration to calculate the time history response when the plate was subjected to a step uniform pressure. A lumped mass discretization was employed.

In order to assess the effect of the lumped mass matrix on the integration step (Δt), the smallest period of the finite element model was calculated using a consistent mass matrix and a lumped mass matrix; we obtained

$$\frac{T_{min}^{LUMPED}}{T_{min}^{CONSIST.}} = 1.1 \ .$$

For the transient solution we used the material-nonlinear-only formulation and $\Delta t = 2 \times 10^{-6}$. Figure 16 compares predicted vertical displacement of the center of the plate with the solutions given in [3].

5. CONCLUSIONS

A new four-node non-flat general nonlinear shell element has been presented with the following important element properties:

- The element is formulated using three-dimensional continuum mechanics theory; hence, the use of the element is not restricted by application of a specific shell theory.
- The element is reliable and has good predictive capability in the analysis of thick and thin shells.
- The amount of computations required to calculate the element stiffness matrix are very closely those that are used in standard isoparametric formulations. The computer time used could be reduced considerably in elastic analysis by using analytical integration through the element thickness.

In this paper we have presented the formulation and some applications of the element. The solution results obtained are most encouraging, but a formal mathematical convergence study of the element would be very valuable, and we are currently pursuing such research.

Finally, it should be noted that the element presented here provides a very attractive basic formulation that could be extended to large strain analysis and analysis of composite shells. Also, the concepts applied here to formulate a 4-node element could equally well be employed in an effective manner to formulate higher-order shell elements.

REFERENCES

1. A. Adini, "Analysis of Shell Structures by the Finite Element Method," Ph.D. Dissertation, Department of Civil Engineering, University of California, Berkeley, California (1961).

2. K.J. Bathe, Finite Element Procedures in Engineering Analysis, Prentice-Hall, Englewood Cliffs, New Jersey (1982).

3. K.J. Bathe and S. Bolourchi, "A Geometric and Material Nonlinear Plate and Shell Element," J. Computers and Structures, Vol. 11, 23-48 (1979).

4. K.J. Bathe and E.N. Dvorkin, "On the Automatic Solution of Nonlinear Finite Element Equations," J. Computers and Structures, Vol. 17, No. 5-6, 871-879 (1983).

5. K.J. Bathe, E.N. Dvorkin and L.W. Ho, "Our Discrete-Kirchhoff and Isoparametric Shell Elements for Nonlinear Analysis — An Assessment," J. Computers and Structures, Vol. 16, No. 1-4, 89-98 (1983).

6. K.J. Bathe and L.W. Ho, "A Simple and Effective Element for Analysis of General Shell Structures," J. Computers and Structures, Vol. 13, 673-682 (1980).

7. K.J. Bathe and L.W. Ho, "Some Results in the Analysis of Thin Shell Structures," Nonlinear Finite Element Analysis in Structural Mechanics, (Edited by W. Wunderlich et al.), Springer-Verlag, Berlin (1981).

8. J.L. Batoz, K.J. Bathe and L.W. Ho, "A Study of Three-Node Triangular Plate Bending Elements," Int. J. Numerical Meth. Eng. Vol. 15, 1771-1812 (1980).

9. J.L. Batoz and M. Ben Tahar, "Evaluation of a New Quadrilateral Plate Bending Element," Int. J. Numerical Meth. Eng., Vol. 18, 1655-1677 (1982).

10. M. Bercovier, Y. Hasbani, Y. Gilon and K.J. Bathe, "On a Finite Element Procedure for Nonlinear Incompressible Elasticity," Hybrid and Mixed Finite Element Methods, (Edited by S.M. Atluri, et al.), John Wiley & Sons (1983).

11. W. Flügge, Stresses in Shells (2nd Edition), Springer-Verlag (1973).

12. K. Forsberg and R. Hartung, "An Evaluation of Finite Difference and Finite Element Techniques for Analysis of General Shells," Symposium on High Speed Computing of Elastic Structures, I.U.T.A.M., Liège (1970).

13. Y.C. Fung, Foundations of Solid Mechanics, Prentice-Hall, Englewood Cliffs, New Jersey (1965).

14. R.H. Gallagher, "Problems and Progress in Thin Shell Finite Element Analysis," Finite Elements in Thin Shells and Curved Members, (Edited by D.G. Ashwell and R.H. Gallagher), John Wiley & Sons (1976).

15. A.E. Green and W. Zerna, Theoretical Elasticity (2nd Edition), Oxford University Press (1968).

16. G. Horrigmoe, "Finite Element Instability Analysis of Free-Form Shells," Report 77-2, Division of Structural Mechanics, The Norwegian Institute of Technology. The University of Trondhein, Norway (1977).

17. T.J.R. Hughes and W.K. Liu, "Nonlinear Finite Element Analysis of Shells: Part I, Three-Dimensional Shells," J. Computer Meth. Appl. Mech. Eng., Vol. 26, 331-362 (1981).

18. B.M. Irons and A. Razzaque, "Experience with the Patch Test for Convergence of Finite Elements," The Mathematical Foundations of the Finite Element Method with Applications to Partial Differential Equations, (Edited by A.K. Aziz), Academic Press (1972).

19. B. Kråkeland, "Nonlinear Analysis of Shells Using Degenerate Isoparametric Elements," Finite Elements in Nonlinear Mechanics, Vol. 1, (Edited by P.G. Bergan et al.), Tapir Publishers (Norwegian Institute of Technology, Trondheim, Norway) (1978).

20. R.H. Leicester, "Finite Deformations of Shallow Shells," Proc. A.S.C.E., Vol. 94, EM6, 1409-1423 (1968).

21. G.M. Lindberg, M.D. Olson and G.R. Cowper, "New Developments in the Finite Element Analysis of Shells," Quarterly Bulletin of the Divisions of Mech. Eng. and the National Aeronautical Establishment, National Research Council of Canada, Vol. 4 (1969).

22. R.H. MacNeal, "A Simple Quadrilateral Shell Element," J. Computers and Structures, Vol. 8, 175-183 (1978).

23. A.K. Noor and J.M. Peters, "Mixed Models and Reduced/Selective Integration Displacement Models for Nonlinear Analysis of Curved Beams," Int. J. Num. Meth. Eng., Vol. 17, 615-631 (1981).

24. E. Ramm and J.M. Sattele, "Elasto-Plastic Large Deformation Shell Analysis Using Degenerated Elements," Nonlinear Finite Element Analysis of Plates and Shells, (Edited by T.J.R. Hughes), A.S.M.E., AMD-Vol. 48, (1981).

25. Report AE 83-5, ADINA System Verification Manual, ADINA Engineering, Västerås, Sweden and Watertown, Mass., June 1983.

26. S.P. Timoshenko and J.M. Gere, Theory of Elastic Stability (2nd Edition), McGraw-Hill (1961).

27. K. Washizu, Variational Methods in Elasticity and Plasticity, Pergamon Press (1968).

28. G. Wempner, D. Talaslidis and C.-M. Hwang, "A Simple and Efficient Approximation of Shells via Finite Quadrilateral Elements," J. Appl. Mechs., Vol. 49, 115-120 (1982).

29. O.C. Zienkiewicz, The Finite Element Method, McGraw-Hill (1977).

DISTRIBUTION LIST

No. of Copies	Organization
12	Administrator Defense Technical Info Center ATTN: DTIC-DDA Cameron Station Alexandria, VA 22314
1	Director of Defense Research & Engineering ATTN: DD/TWP Washington, DC 20301
1	Asst. to the Secretary of Defense (Atomic Energy) ATTN: Document Control Washington, DC 20301
1	Director Defense Advanced Research Projects Agency ATTN: Tech Lib 1400 Wilson Boulevard Arlington, VA 22209
2	Director Federal Emergency Management Agency ATTN: Mr. George Sisson/RF-SR Technical Library Washington, DC 20301
1	Director Defense Intelligence Agency ATTN: DT-2/Wpns & Sys Div Washington, DC 20301
1	Director National Security Agency ATTN: E. F. Butala, R15 Ft. George G. Meade, MD 20755
1	Director Joint Strategic Target Planning Staff JCS Offut AFB Omaha, NB 68113
1	HQDA DAMA-ART-M Washington, DC 20310
1	Director Defense Communications Agency ATTN: 930 Washington, DC 20305
11	Director Defense Nuclear Agency ATTN: DDST/Dr. Conrad SPAS/P. R. Rohr SPSS/K. Goering G. Ullrich SPTD/T. Kennedy SSTL/Tech Lib (2 cys) STSI/Archives STSP/COL Kovel NATD NATA Washington, DC 20305
2	Commander Field Command, DNA ATTN: FCPR FCTMOF Kirtland AFB, NM 87115
1	Commander Field Command, DNA Livermore Branch ATTN: FCPRL P.O. Box 808 Livermore, CA 94550
1	Director Inst for Defense Analyses ATTN: IDA Librarian Ruth S. Smith 400 Army-Navy Drive Arlington, VA 22202
1	Commander US Army Materiel Command ATTN: AMCDRA-ST 5001 Eisenhower Avenue Alexandria, VA 22333

DISTRIBUTION LIST

No. of Copies	Organization
1	Program Manager US Army BMD Program Office ATTN: John Shea 5001 Eisenhower Avenue Alexandria, VA 22333
2	Director US Army BMD Advanced Technology Center ATTN: CRDABH-X CRDABH-S Huntsville, AL 35807
1	Commander US Army BMD Command ATTN: BDMSC-TFN/N.J. Hurst P.O. Box 1500 Huntsville, AL 35807
1	Commander US Army Engineer Division ATTN: HNDED-FD P.O. Box 1600 Huntsville, AL 35807
2	Deputy Chief of Staff for Operations and Plans ATTN: Technical Library Director of Chemical & Nuc Operations Department of the Army Washington, DC 20310
2	Office, Chief of Engineers Department of the Army ATTN: DAEN-MCE-D DAEN-RDM 890 South Pickett Street Alexandria, VA 22304
3	Commander US Army Engineer Waterways Experiment Station ATTN: Technical Library William Flathau Leo Ingram P.O. Box 631 Vicksburg, MS 39180
1	Commander US Army Engineering Center ATTN: ATSEN-SY-L Fort Belvoir, VA 22060
1	US Army MERADCOM ATTN: DRDME-EM, D. Frink Fort Belvoir, VA 22060
1	Commander US Army Armament Research and Development Center ATTN: SMCAR-TDC Dover, NJ 07801
1	Commander US Army Armament Research and Development Center ATTN: SMCAR-TSS Dover, NJ 07801
1	Commanmder US Army Armament Materiel Readiness Command ATTN: AMSMC-LEP-L, Rock Island, IL 61299
1	Director Benet Weapons Laboratory US Army Armament Research and Development Center ATTN: SMCAR-LCB-TL Watervliet, NY 12189
1	Commander US Army Aviation Research and Development Command ATTN: AMSAV-E 4300 Goodfellow Boulevard St. Louis, MO 63120
1	Director US Army Air Mobility Research and Development Laboratory Ames Research Center Moffett Field, CA 94035

DISTRIBUTION LIST

No. of Copies	Organization
2	Commander US Army Communications Rsch and Development Command ATTN: AMSEL-ATDD AMSEL-PPA-SA Fort Monmouth, NJ 07703
3	Commander US Army Electronics Research and Development Command Technical Support Activity ATTN: AMDSD-L AMDEW-E, W. S. McAfee AMDSD-EI, J. Roma Fort Monmouth, NJ 07703
8	Commander US Army Harry Diamond Labs ATTN: Mr. James Gaul Mr. L. Belliveau Mr. J. Meszaros Mr. J. Gwaltney Mr. F. W. Balicki Mr. Bill Vault Mr. R. J. Bostak Mr. R. K. Warner 2800 Powder Mill Road Adelphi, MD 20783
4	Commander US Army Harry Diamond Labs ATTN: DELHD-TA-L DRXDO-TI/002 DRXDO-NP DELHD-RBA/J. Rosado 2800 Powder Mill Road Adelphi, MD 20783
1	Commander US Army Infantry School ATTN: ATSH-CD-CSO-OR Fort Benning, GA 31905
1	Commander US Army Missile Command ATTN: AMSMI-R Redstone Arsenal, AL 35898
1	Commander US Army Missile Command ATTN: AMSMI-YDL Redstone Arsenal, AL 35898
1	Commander US Army Missile Command ATTN: Technical Library Redstone Arsenal, AL 35898
4	Commander US Army Natick Research and Development Command ATTN: DRDNA-DT Dr. D. Sieling DRXNE-UE/A. Johnson A. Murphy W. Crenshaw Natick, MA 01760
1	Commander US Army Tank Automotive Command ATTN: AMSTA-TSL Warren, MI 48090
1	Comander US Army Foreign Science and Technology Center ATTN: Rsch & Cncepts Br 220 7th Street , NE Charlottesville, VA 22901
1	Commander US Army Logistical Center ATTN: ATCL-SCA Mr. Robert Cameron Fort Lee, VA 23801
3	Commander US Army Materials and Mechanics Research Center ATTN: Technical Library DRXMR-ER, Joe Prifti Eugene de Luca Watertown, MA 02172

DISTRIBUTION LIST

No. of Copies	Organization
1	Commander US Army Research Office P.O. Box 12211 Research Triangle Park NC 27709
4	Commander US Army Nuclear Agency ATTN: ACTA-NAW MONA-WE Technical Library MAJ Uecke 7500 Backlick Rd, Bldg. 2073 Springfield, VA 22150
1	Commander US Army TRADOC ATTN: ATCD-SA, Mr. O. Wells Fort Monroe, VA 23651
1	Director US Army TRADOC Systems Analysis Activity ATTN: LTC John Hesse ATAA-SL, Tech Lib White Sands Missile Range NM 88002
1	Commander US Combined Arms Combat Developments Activity ATTN: ATCA-CO, Mr. L. C. Pleger Fort Leavenworth, KS 66027
1	Commandant Interservice Nuclear Weapons School ATTN: Technical Library Kirtland AFB, NM 87117
1	Chief of Naval Material ATTN: MAT 0323 Department of the Navy Arlington, VA 22217
2	Chief of Naval Operations ATTN: OP-03EG OP-985F Department of the Navy Washington, DC 20350
1	Chief of Naval Research ATTN: N. Perrone Department of the Navy Washington, DC 20360
1	Director Navy Strategic Systems Projects Ofc ATTN: NSP-43, Tech Library Department of the Navy Washington, DC 20360
1	Commander Naval Electronic Systems Com ATTN: PME 117-21A Washington, DC 20360
1	Commander Naval Facilities Engineering Command Washington, DC 20360
1	Commander Naval Sea Systems Command Department of the Navy Washington, DC 20360
3	Officer-in-Charge (Code L31) Civil Engineering Laboratory Naval Constr Btn Center ATTN: Stan Takahashi R. J. Odello Technical Library Port Hueneme, CA 93041
1	Commander David W. Taylor Naval Ship Research & Development Ctr ATTN: Lib Div, Code 522 Bethesda, MD 20084

DISTRIBUTION LIST

No. of Copies	Organization
1	Commander Naval Surface Weapons Center ATTN: DX-21, Library Br. Dahlgren, VA 22448
2	Commander Naval Surface Weapons Center ATTN: Code WA501/Navy Nuclear Programs Office Code WX21/Tech Library Silver Spring, MD 20910
1	Commander Naval Weapons Center ATTN: Code 3433 Tech Lib China Lake, CA 93555
1	Commander Naval Weapons Evaluation Fac ATTN: Document Control Kirtland AFB, NM 87115
1	Commander Naval Research Laboratory ATTN: Code 2027, Tech Lib Washington, DC 20375
1	Superintendent Naval Postgraduate School ATTN: Code 2124, Technical Reports Library Monterey, CA 93940
1	AFSC (Tech Lib)/SDOA Andrews Air Force Base Washington DC 20334
1	ADTC (Tech Lib) Eglin AFB, FL 32542
1	AFATL (DLYV) Eglin AFB, FL 32542
1	RADC (EMTLD/Docu Libray) Griffiss AFB, NY 13441

No. of Copies	Organization
1	AFWL/NTES (R. Henny) Kirtland AFB, NM 87117
1	AFWL/NTE, CPT J. Clifford Kirtland AFB, NM 87117
1	AFWL/SUL Kirtland AFB, NM 87115
1	Commander-in-Chief Strategic Air Command ATTN: NRI-STINFO Lib Offutt AFB, NB 68113
1	AFIT (Lib Bldg. 640, Area B) Wright-Patterson AFB Ohio 45433
1	FTD (TD/BTA/Lib) Wright-Patterson AFB Ohio 45433
1	Director Lawrence Livermore Lab. ATTN: Tech Info Dept L-3 P.O. Box 808 Livermore, CA 94550
1	Director Los Alamos Scientific Lab ATTN: Doc Control for Rpts Lib P.O. Box 1663 Los Alamos, NM 87544
2	Director Sandia National Laboratory ATTN: Doc Control for 3141 Sandia Rpt Collection L. J. Vortman Albuquerque, NM 87115
1	Commander US Army Development & Employment Agency ATTN: MODE-TED-SAB Fort Lewis, WA 98433

DISTRIBUTION LIST

No. of Copies	Organization
1	Director Sandia Laboratories Livermore Laboratory ATTN: Doc Control for Tech Lib P.O. Box 969 Livermore, CA 94550
1	Director National Aeronautics and Space Administration Scientific & Tech Info Fac P.O. Box 8757 Baltimore/Washington International Airport MD 21240
1	Aerospace Corporation ATTN: Tech Info Services P.O. Box 92957 Los Angeles, CA 90009
1	Agbabian Associates ATTN: M. Agbabian 250 North Nash Street El Segundo, CA 90245
1	The BDM Corporation ATTN: Richard Hensley P.O. Box 9274 Albuquerque International Albuquerque, NM 87119
1	The Boeing Company ATTN: Aerospace Library P.O. Box 3707 Seattle, WA 98124
2	California Research and Technology ATTN: M. Rosenblatt F. Sauer 20943 Devonshire Street Chatsworth, CA 91311
1	Carpenter Research Corporation ATTN: H. Jerry Carpenter 6230 Scotmist Drive Rancho Palos Verdes, CA 90274
1	Goodyear Aerospace Corp ATTN: R. M. Brown, Bldg 1 Shelter Engineering Litchfield Park, AZ 85340
2	Kaman AviDyne ATTN: Dr. N.P. Hobbs Mr. S. Criscione 83 Second Avenue Northwest Industrial Park Burlington, MA 01803
3	Kaman Sciences Corporation ATTN: Library P. A. Ellis, F. S. Shelton P.O. Box 7463 1500 Garden of the Gods Road Colorado Springs, CO 80907
1	Kaman Sciences Corporation ATTN: Don Sachs Suite 703 2001 Jefferson Davis Highway Arlington, VA 22202
1	Kaman-TEMPO ATTN: DASIAC P.O. Drawer QQ Santa Barbara, CA 93102
1	Kaman-TEMPO ATTN: E. Bryant, Suite UL-1 715 Shamrock Road Bel Air, MD 21014
1	Lockheed Missiles & Space Co. ATTN: J. J. Murphy, Dept. 81-11, Bldg. 154 P.O. Box 504 Sunnyvale, CA 94086

DISTRIBUTION LIST

No. of Copies	Organization
1	Martin Marietta Corporation Aerospace Division ATTN: G. Fotieo P.O. Box 5837 Orlando, FL 32805
2	McDonnell Douglas Astronautics Corporation ATTN: Robert W. Halprin Dr. P. Lewis 5301 Bolsa Avenue Huntington Beach, CA 92647
2	The Mitre Corporation ATTN: Library J. Calligeros, Mail Stop B-150 P.O. Box 208 Bedford, MA 01730
1	New Mexico Engineering Research Institute (CERF) ATTN: J. Leigh P.O. Box 25 UNM Albuquerque, NM 87131
1	Radkowski Associates ATTN: Peter R. Radkowski P.O. Box 5474 Riverside, CA 92517
2	Physics International ATTN: Technical Library Mr. Fred Sauer 2700 Merced Street San Leandro, CA 94577
2	Union Carbide Corporation Holifield National Laboratory ATTN: Doc Control for Tech Lib Civil Defense Research Project P.O. Box X Oak Ridge, TN 37830
3	R&D Associates ATTN: Jerry Carpenter Technical Library Allan Kuhl P.O. Box 9695 Marina del Rey, CA 90291
1	RCA Government Communications Systems 13-5-2 Front & Cooper Streets Camden, NJ 08102
2	Science Applications, Inc. ATTN: Burton S. Chambers John Cockayne PO BOX 1303 1710 Goodridge Drive McLean, VA 22102
1	Science Applications, Inc. ATTN: Technical Library PO Box 2351 La Jolla, CA 92038
1	Systems, Science and Software ATTN: C. E. Needham PO Box 8243 Albuquerque, NM 87108
3	Systems, Science and Software ATTN: Technical Library R. Duff K. Pyatt PO Box 1620 La Jolla, CA 92037
1	TRW Electronics and Defense ATTN: Benjamin Sussholtz One Space Park Redondo Beach, CA 92078

DISTRIBUTION LIST

No. of Copies	Organization
1	Washington State University Physics Department ATTN: G. R. Fowles Pullman, WA 99163
1	Battelle Memorial Institute ATTN: Technical Library 505 King Avenue Columbus, OH 43201
1	California Inst of Tech ATTN: T. J. Ahrens 1201 E. California Blvd. Pasadena, CA 91109
2	Denver Research Institute University of Denver ATTN: Mr. J. Wisotski Technical Library PO Box 10127 Denver, CO 80210
1	IIT Research Institute ATTN: Milton R. Johnson 10 West 35th Street Chicago, IL 60616
1	TRW Systems Group Ballistic Missile Division ATTN: H. Korman, Mail Station 526/614 P.O. Box 1310 San Bernardino CA 92402
1	J. D. Haltiwanger Consulting Services B106a Civil Engineering Bldg. 208 N. Romine Street Urbana, IL 61801
1	Massachusetts Institute of Technology Aeroelastic and Structures Research Laboratory ATTN: Dr. E. A. Witmer Cambridge, MA 02139
2	Massachusetts Institute of Technology Mechanical Engineering Dept. ATTN: Prof. K. J. Bathe Dr. Eduardo N. Dvorkin Cambridge, MA 02139
2	Southwest Research Institute ATTN: Dr. W. E. Baker A. B. Wenzel 8500 Culebra Road San Antonio, TX 78228
1	SRI International ATTN: Dr. G. R. Abrahamson 333 Ravenswood Avenue Menlo Park, CA 94025
1	Stanford University ATTN: Dr. D. Bershader Durand Laboratory Stanford, CA 94305

Aberdeen Proving Ground

Dir, USAMSAA
ATTN: AMXSY-D
AMXSY-MP, H. Cohen
Cdr/USATCOM
ATTN: AMSTE-TO-F
Cdr/CRDC, AMCCOM
ATTN: SMCCR-RSP-A
SMCCR-MU
SMCCR-SPS-IL